4. VISUALIZATION OF NANOSTRUCTURES WITH ATOMIC FORCE MICROSCOPY

SERGEI N. MAGONOV AND NATALYA A. YERINA

INTRODUCTORY REMARKS

Scanning tunneling microscopy (STM) and Atomic Force Microscopy (AFM) were introduced about 20 years ago [1, 2]. Since this time these techniques have revolutionized surface analysis by providing high-resolution visualization of structures at the atomic- and nanometer-scales. The remarkable feature of STM and AFM instruments is their ability to examine samples not only in an ultrahigh vacuum but also at ambient conditions and even in liquids. In both methods, the localized interaction between a sharp probe and a sample is employed for surface imaging. STM is based on detection of tunneling current between a sharp metallic tip and a conducting surface. This circumstance limits STM applications, and it is applied mostly to studies of atomic structures and atomic-scale processes on different conducting and semiconducting samples, primarily in UHV conditions. Therefore, the use of STM is confined to research laboratories at Universities and Government Institutions dealing with fundamental problems of surfaces, whereas industrial laboratories are using AFM exclusively which can be applied for characterization of materials of any kind. This functionality is inherent to AFM, which is based on detection of more universal tip-sample mechanical forces.

The scope of AFM applications includes high-resolution examination of surface topography, compositional mapping of heterogeneous samples and studies of local mechanical, electric, magnetic and thermal properties. These measurements can be performed on scales from hundreds of microns down to nanometers, and the importance

of AFM, as characterization technique, is further increasing with recent developments in nanoscience and nanotechnology. In studies of surface roughness, AFM complements optical and stylus profilometers by extending a measurement range towards the sub-100 nm scale and to forces below nanoNewton. These measurements are valuable in several industries such as semiconductors, data storage, coatings, etc. AFM together with scanning electron microscopy of critical dimensions is applied for examination of deep trenches and under-cut profiles with tens and hundreds of nanometers dimensions, which are important technological profiles of semiconductor manufacturing. AFM capability of compositional imaging of heterogeneous polymer systems (blends, block copolymers, composites, filled rubbers) attracts the attention of researchers working in industries, which are dealing with synthesis, design and formulation of plastic materials as well as their applications. In this function, AFM assists other microscopic and diffraction techniques (light, X-ray, and neutron scattering). Nanoscale objects such as mineral and organic filler particles, carbon nanotubes or individual macromolecules of biological and synthetic origin are distinguished in AFM images. Studies of these objects and their self-assemblies on different substrates are addressing important problems of intermolecular interactions in confined geometries. Better understanding of these interactions and the ways they might be controlled are needed for a preparation of functional surfaces, nano-scale patterning and manipulation of nanoscale objects.

Local probing of mechanical properties is another important function of AFM that offers unique capabilities for studies of structure-property relationships at the nanometer scale. A recording of force curves and performing nanoindentation at surface locations of tens of nanometers in size are routinely employed for such measurements. At present, this is only a comparative analysis of mechanical responses of different samples or different sample components. In addition to mechanical properties, examination of local electric properties at the sub-micron scales will be welcomed by many applications. Electric force microscopy, which is most known AFM technique for mapping of conducting regions of various samples, is based on measurements of electric field gradients acting between a metal-coated probe and conducting sample regions. Detection of local electric properties such as current-voltage characteristics of the nanoscale objects is a more challenging task and requires substantial instrumental improvements to became a routine procedure.

At present AFM became a mature characterization technique that is in permanent development. Intensive efforts are underway in AFM instrumentation and its applications. The design of novel probes with various geometries and unique dynamic properties has already enhanced the technique's dynamic capabilities, mechanical measurements and image resolution. The use of piezoceramic actuators as scanners in AFM instruments has such drawbacks as non-linearity and creep, which are related to polycrystalline nature of these materials. An introduction of high-precision scanners based on closed-loop positioning systems is addressing this problem. The recognized AFM limitation is its low efficiency due to slow scanning. The development of new approaches to fast scanning will enable high throughput capabilities of imaging and screening for combinatorial approaches in material science and technology. Nanomechanical measurements become crucial for characterization of

nanomaterials, which offer the promise of breakthrough longstanding limits of material performance. Most importantly, the proper characterization of these materials and their performance is impossible without quantitative studies of nanomechanical properties. Therefore, there are strong incentives for development of reliable approaches toward quantitative nanomechanical analysis. The AFM-based techniques (nanoindentation, scratching, etc.) have intrinsic advantages for overcoming fundamental difficulties of indenters, which are routinely used for micro-mechanical testing, and which are not suitable at scales below a half of micron and for operation at low forces. Various attempts are on the way to make nanomechanical measurements with AFM more quantitative, with unique spatial resolution and also to provide such measurements in broad frequency range.

This chapter presents a short review of contemporary AFM and main issues related to its instrumentation and practical imaging at the nanometer scale. AFM applications will be illustrated by examples taken from studies of single macromolecules and their self-assemblies on different surfaces and compositional mapping of semicrystalline polymers, block copolymers, polymer blends and composites. The choice of practical examples reflects the fact that AFM studies of polymers are the field most familiar to the authors.

BASICS OF ATOMIC FORCE MICROSCOPY

Main Principle and Components of Atomic Force Microscope

In AFM, mechanical force interactions acting between a sharp probe and a sample are used for surface imaging. The probe, which represents a micromachined cantilever with a sharp tip at one end, is brought into interaction with the sample surface. The interaction level between the tip apex and the sample is determined through precise measurements of the cantilever displacements. Initial attempts to apply STM for gauging the cantilever deflection had little success. An optical level detection, which had been originally suggested for gravimeters [3], appeared invaluable for precise measurements of the cantilever deflection in most commercial atomic force microscopes [4]. In this procedure, a laser beam, which is deflected from the backside of the cantilever, is directed to a 4-segment positional photodetector, which is divided into segments for measurements of normal and lateral deflections of the cantilever. At present, the optical level detection is the most reliable way to measure the tip-sample force interactions, Figures 1a–b. This approach does not completely free of problems related with the use of light, such as parasitic interference at the cantilever-sample confinement, heating of a cantilever and a sample by the laser beam. Therefore, the microscope designers are looking for alternative approaches. Among them is the AFM based on a microfabricated piezocantilever, in which the cantilever itself provides not only the deflection sensing but also the actuation [5].

The surface imaging is realized by detecting the tip-sample force in different locations while the probe is rastering the sample surface with the help of a piezoelectric actuator. A feedback control applied during imaging ensures that the tip-sample force is preserved at a constant level. The error signal, which is used for feedback control,

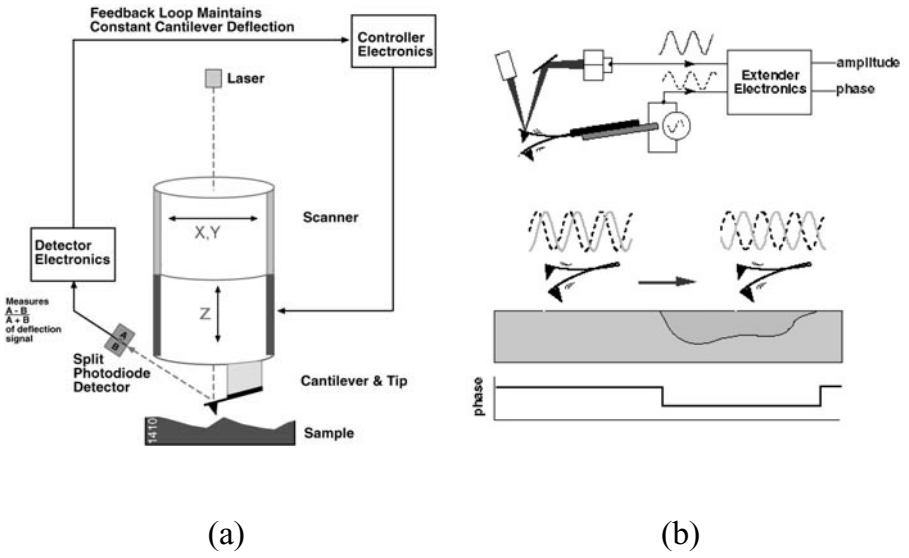

Figure 1. (a) Sketch demonstrating main components of atomic force microscope working in the contact mode in which the tip is permanently engaged into the sample. A cantilever deflection responding to tip-sample forces is measured with the optical lever scheme. (b) Sketch illustrating phase detection and phase imaging in tapping mode. Phase of the probe oscillation changes when an AFM probe comes into interaction with the sample. Phase can be different when the probe interacts with different components of a heterogeneous sample.

is amplified to generate height images, which reflect surface corrugations. The height image, in which brighter contrast is assigned to elevated surface locations, represent the vertical translations of the piezo-scanner needed to eliminate the error signal when the probe is moved from one sample location to the other. The error signal images, which, might be considered as maps of derivatives of height corrugations, emphasize fine surface features that are poor resolved in the height images.

From a brief description of the method it becomes clear that the main components of atomic force microscope are probes, optical detection system, piezo-scanners and electronics for a management of scanning procedures and data acquisition, Figures 1a–b. In the microscope, these components are assembled into a microscope stage, which must satisfy the requirements of minimum vibrational, acoustic and electronic noise as well as small thermal drift. Basic information about these components could be useful for better understanding the performance of AFM instruments, their unique features and limitations.

Scanners, which are applied for 3D movement of the sample or probe in AFM, are made of piezoelectric materials, which provide the precise positioning and ability to transport the objects in the micron range with sub-angstrom precision. Yet due to polycrystalline nature of these materials, the motion of real scanners deviates from linear dependence on applied voltage, especially at voltages generating large translations. In

addition, the motion along the different axes is not completely independent. Therefore, a careful design, precise construction and calibration are important objectives that should be addressed during manufacturing of the scanners and their use. These efforts will allow the real scanners to approach a desirable performance, yet an additional electronic control is still needed. In an open-loop scanner, the controller drives the scanner using a non-linear voltage profile that produces a linear motion. This profile is taught during the calibration procedure on surface gratings with the known pitch in lateral dimensions and height steps in vertical direction, Figures 2a–b. Such calibration has limited precision because the scanner response to a particular voltage depends on the material history. Minimal distortions are expected when scanning is performed at the small range near the scanner rest point and the distortions will increase substantially when high voltages are applied for large-scale scanning. The situation is worse when the scanner is applied for small scans far away from the rest point immediately after its use for large scans.

To address the open-loop control problems, the scanner can be fitted with independent position sensors. In this case of a closed-loop system, the controller reads the sensor outputs and adjusts the drive voltage in order to achieve the desired motion. The microscopes with the closed-loop control of the scanners became popular recently to address problems of object manipulation, surface lithography and patterning in the micron and sub-micron scales. It is worth noting that despite the improved precision of the probe or sample translation the performance of the closed-loop systems is subjected to influence of thermal drift and additional noise that hurts quality of high-resolution imaging. Scan accuracy of both systems (open-loop and close-loop) depends on their calibration using appropriate standards. Man-made standards are available for the lateral scales of hundreds of nanometers and larger, Figures 2a–b. For calibration at the nanometer and atomic scale, one can apply periodical patterns of natural materials such as alkanes and the lattice spacing of crystalline surfaces of mica and highly-ordered pyrolitic graphite, Figures 2c–d.

AFM has been introduced for visualization of structures at the atomic-scale. However, with development of its applications the technique became useful for many other purposes and the size of the samples and structures to be examined has varied tremendously. This need led to the development of AFM instruments that can be used for studies of large objects (e.g. 12-inch Si wafers) with the instrument operation fully automated. In the automated microscopes, in addition to piezoscanners, different translation XY stages are applied. In addition to motorized stages, flexure stages are also used in AFM instruments. The flexure stages are closer to the performance of piezo-scanners and offer some additional capabilities. The close-loop flexure stages are also developed for commercial microscopes.

An introduction of microfabricated Si_3N_4 and Si probes, which consists of the cantilevers with a sharp tip at one end that can be prepared in batch processes, was one of the key events that led to the broad use of AFM instruments. Major parameters of the AFM probes are the cantilever shape and stiffness, oscillatory parameters (resonance frequency, Q-factor), tip geometry (a shape and size of its apex), and specific functionality.

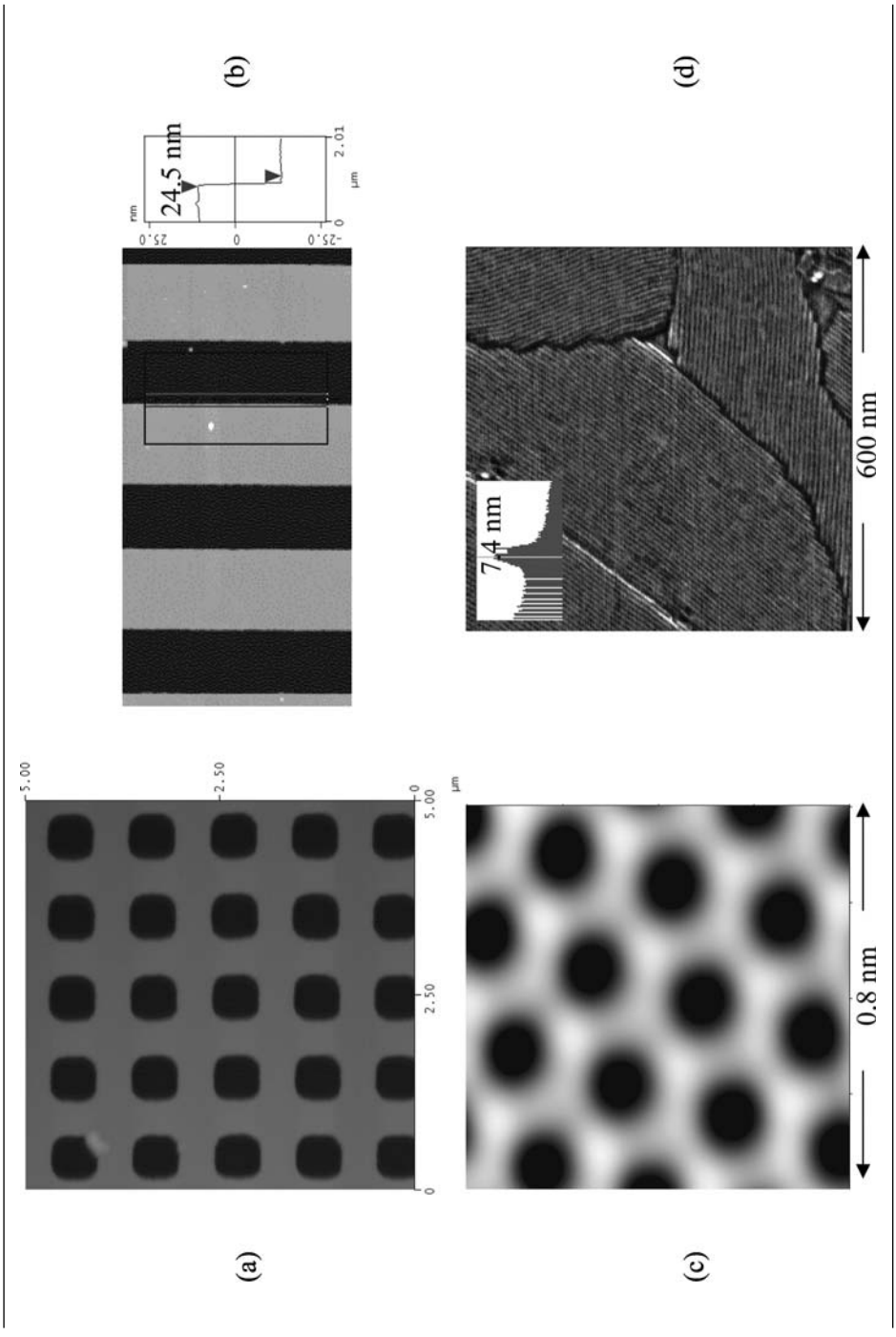
(a)
5.00
2.50
0
5.00
2.50
0
µm
(b)
24.5 nm
25.0
0
-25.0
nm
2.01
µm
0
(c)
0.8 nm
(d)
7.4 nm
600 nm

Most of the probes have rectangular or triangular cantilevers and a sharp pyramidal tip at the end. Practically, it is more feasible to make thinner and softer cantilevers out of S_3N_4. Therefore these probes, which are traditionally made with triangular cantilevers, are applied for studies of soft biological samples and are used primarily for contact mode measurements in air and under water. Stiffness of Si_3N_4 probes depends on dimensions of the triangular cantilevers and varies in the 0.01 N/m–0.6 N/m range. Si probes usually have rectangular cantilevers and the range of stiffness is much broader: from 0.1 N/m to 400 N/m. The softest probes can be used for the contact mode measurements whereas tapping mode [6] imaging requires stiffer probes because one should be able to retract the probe from a sample in every cycle of its oscillation. This can be achieved only with probes whose stiffness overcomes adhesive interactions with the sample.

Before an experiment it might be quite difficult to determine what minimal stiffness of the probe is needed for successful measurements of a particular sample. For studies of soft materials (polymers and biological objects), a broad range of probes can be used. On one hand, softer probes will facilitate gentle imaging of these materials. On another hand, visualization of the composition of the heterogeneous samples with high contrast requires the probe with optimal stiffness. Therefore, the probes, whose stiffness varies in the range from 0.1 N/m to 400 N/m, can be employed for compositional mapping. This is related to the fact that stiffness of polymeric materials differs in a broad range and matching the probe stiffness to that of a polymer sample or its different components helps to visualize individual components of multicomponent materials. The probe choice also depends on the operation mode and environmental conditions. For imaging in air, Si probes with stiffness of 3–5 N/m are most useful, especially when high-resolution and low-force imaging is required. For compositional imaging, which is commonly conducted at elevated tip-forces, Si probes with stiffness 30–40 N/m will be a good choice. Imaging under liquids can be done with soft Si probes (0.3–1 N/m). The resonant frequency and Q-factor of the probes are essential dynamic parameters that influence the scanning rate of imaging in oscillatory modes and soft probes with high-resonance frequency are ideal for fast scanning of biological objects.

Tip geometry is the crucial parameter for many AFM applications such as measurements of narrow trenches and rectangular surface steps, profiling of single lying objects, as well as visualization of atomic-scale features on crystalline surfaces. The overall shape of Si_3N_4 tip is a square pyramid with the half-angles of its faces $\sim 35^\circ$. The nominal radius of curvature at the tip is <20 nm. Si probes are etched in the shape of an irregular pyramid with the nominal apex radius <10 nm. Near the apex the shank is triangular with the half angles of 17° (sides), 25° (front), and 10° (rear),

←

Figure 2. (a)–(b) Height images of the calibration standards for lateral (X, Y) and vertical (Z) directions, respectively. (c) STM image of highly ordered pyrolitic graphite. (d) Phase image of normal alkane $C_{60}H_{122}$ layer on graphite. The insert in the top left corner shows the power spectral density plot and a value of the most pronounced peak, which corresponds to the length of the alkane molecules in the extended all-trans conformation.

where the "front" is closest to the end of the cantilever. For critical measurements of surface features one should consider the absolute orientation of the sample surface and tip to avoid an incorrect judgment. The quality of commercial AFM probes might vary, therefore, for reliable imaging one can preliminary check the probes by imaging test samples such as Au colloid spheres on a smooth substrate, ridged structures of the $SrTiO_3$ (305) surface, edges of the TiO_2 surface, and sharp pyramids. Special care should be exercised during such measurements to avoid undesirable tip damage.

The described probes are most common in routine AFM applications, and the tip apex size of Si probe is one of the factors determining the imaging resolution in tapping mode. Therefore, there are ongoing efforts of design and manufacturing of novel probes with sharp extremities. Two kinds of new probes [7, 8], which might be useful for high-resolution imaging, are shown in Figures 3a–b. The first one was prepared by plasma-assisted deposition of carbon materials on the apex of Si tip. The probe of the second type has a diamond tip with a mechanically sharpened apex. The radius of the curvature at the end of these probes is approaching 1 nm. Recent results demonstrated that tapping mode imaging with true molecular resolution could be achieved with the spiky probes [7]. Unfortunately, multiple spikes, which grow at the Si apex, limit the ease-of-use of these probes. The diamond tip does not have this drawback, however the cost of these probes is significantly higher than the probes with spikes that are produced in batch process. Carbon nanotubes with nanometer-scale diameter were also suggested for use as AFM probes, and their fabrication has advanced from a manual assembling to the catalytic growth of nanotubes at the apex of AFM probes [9, 10]. Yet the images obtained with CNT probes so far do not show the resolution improvement. They also show mechanical instabilities that limit the use of the CNT probes.

Probes with specific functionality can be prepared by coating the cantilever or tip with different materials. Metallic coatings are deposited on the cantilevers in order to increase their optical reflectivity and electric conductivity. The probes with ferromagnetic coatings are applied for magnetic force microscopy. Unfortunately, the coating can make the tip apex less sharp. It is worth noting that the AFM probes with piezoelectric coatings might offer exceptional capabilities for this technique in the near future. A possible application of such cantilevers for self-actuation and detection of the tip-sample interactions might eliminate the optical detection and its related restrictions for some AFM applications. The dynamic characteristics of the piezoelectric cantilevers are superior to those of the regular cantilevers, which are driven externally. This circumstance has been utilized in the development of fast scanning mode, which is essential for high efficiency of AFM and high throughput measurements. So far, due to some instrumental and practical hurdles, this approach has not been broadly accepted. Instead it is possible to make use of these cantilevers for dynamic mechanical measurements of polymer samples. The preliminary results show that this approach allows extending the mechanical studies to high frequencies (up to 100 kHz), which are not accessible to conventional dynamic mechanical analysis [11].

For many years, the probes with chemically modified tips were employed for selective detection of surface locations with different chemical properties. Typical chemical

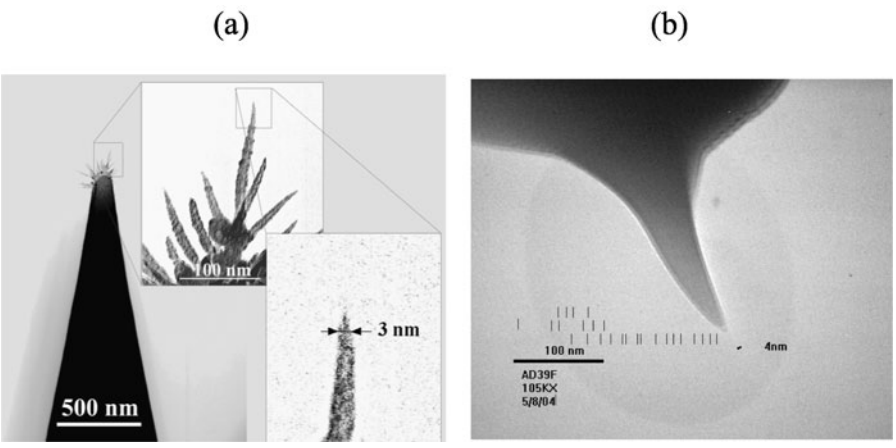

Figure 3. Electron microscopy micrograph of the tips of novel AFM probes. (a) The probe with the carbon spikes (the picture – courtesy of D. Klinov, Institute of Biorganic Chemistry, Moscow, Russia). (b) The diamond probe with a mechanically sharpened apex (the picture – courtesy of B. Mesa, MicroStar Technology, Inc., Huntsville, TX, USA).

modification includes a coating of the tip with a gold layer followed by adsorption of alkylthiols with various functional groups. The use of these modified probes is quite a challenging task. An adequate control of the coating integrity, which might be damaged by tip-sample forces, as well as statistical approaches for data collection and analysis are required for getting reliable results with these probes. Alternatively, AFM probes with different chemical nature can be microfabricated of polymeric materials. Such probes, which are prepared by either etching of photoresist [12] or by extrusion, offer a desirable diversity of the tip material. They also are much softer than the Si and Si_3N_4 probes that facilitate measurements with lower forces.

Concluding the short description of AFM instrumentation it is worthwhile to note the importance of the overall mechanical design of the microscopes, which substantially influence the quality of images. Visualization of the nanoscale structures, particularly in the sub-100 nm scale, essentially depends on the thermal drift of the microscope. Thermal drift harms imaging because the rate of AFM scanning is limited by the physics of tip-sample force interactions and dynamics of the probes, especially, when oscillatory modes are applied. Fast scanning approaches, so far, require an increase of tip-sample interactions that might not be useful for imaging of soft samples. Therefore, special care should be taken to minimize thermal drift by a proper microscope design and rational choice of construction materials for instrument components and enclosures, which are required for acoustic noise isolations. Note that the close-loop scanners are also suffering from thermal drift that limits the value of this approach. An example of imaging with low thermal drift microscope Dimension 5000, in which room temperature drift is as small as 0.5 nm per minute, given in Figures 4a–d. These four images of an array of single macromolecules (polyphenylacetylene with mini-dendritic groups) on graphite were collected in sequential scans of the same area,

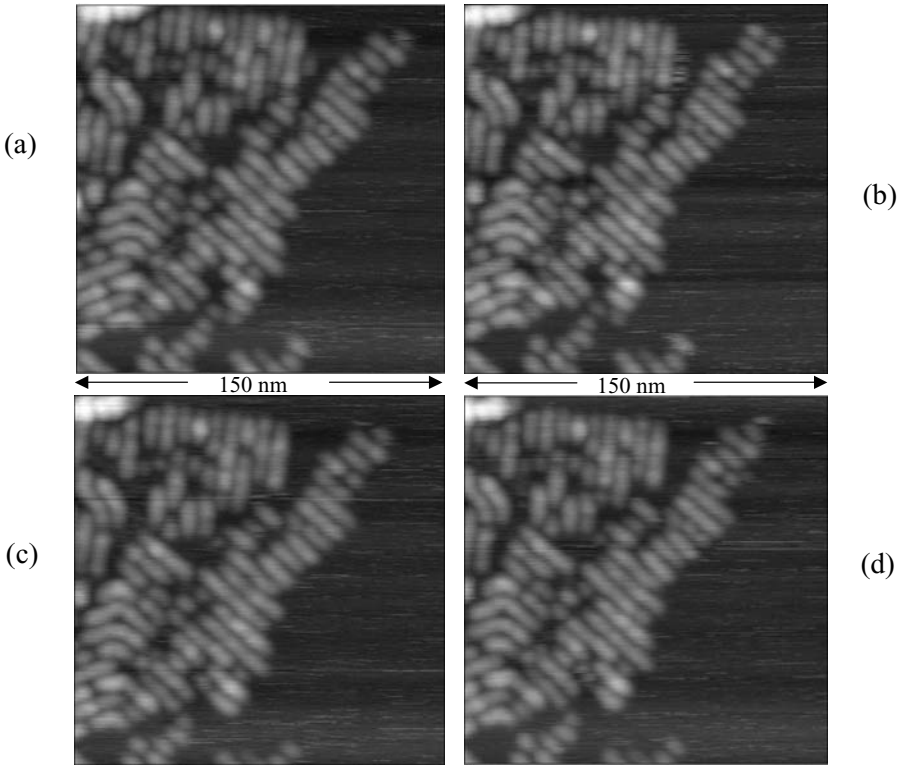

Figure 4a–d. Sequential height images of a stack of single chains of polyphenylacetylene with mini-dendritic groups on graphite.

when the probe was rastering the surface in alternative directions (up to down, down to up, etc.).

Operational Modes, Optimization of the Experiment and Image Resolution

There are two main operation modes in AFM: contact mode and tapping or intermittent contact mode. In the contact mode, which was introduced in practice first, the probe comes into a permanent contact with a sample surface. A product of the cantilever stiffness on its deflection determines the tip-sample force. For many samples, this mode should be applied with caution and the cantilevers with low spring constants are needed for gentle profiling of soft surfaces. Imaging with high-resolution was demonstrated with the contact mode AFM on many crystalline surfaces [13]. Besides surface imaging, AFM in its force modulation mode [14] has been effectively used for evaluation of sample mechanical properties by modulating the tip-force with an additional actuator. Lateral tip-sample forces accompany scanning of surfaces with the tip being in contact, and these forces can be recorded for evaluation of surface friction.

Unfortunately, lateral forces applied to soft samples might induce a strong shearing deformation and sample damage. This limits the contact mode applicability to studies of polymers and biological objects.

In AFM, local tip-sample forces can be measured using deflection-versus-distance curves [15]. These measurements are also helpful for choosing appropriate set-point deflections for surface imaging with different forces. By immersing the sample and the probe in liquid, one can eliminate capillary forces applied to the tip by a liquid contamination layer, which presents on surfaces in air. Therefore, imaging in liquids can be performed at small forces below 1 nN. For biological samples, aqueous media is essential and most of AFM studies of these objects are done underwater. For other materials, imaging in liquids is only an optional, not a routine operation.

This situation changed drastically with the introduction of the AFM oscillatory mode known as the tapping mode [6]. Tapping is performed by the probe, which is driven into oscillatory motion at its resonant frequency by an additional piezoactuator, Figure 1b. A drop of the cantilever amplitude when the tip comes into interaction with a sample is used as a measure of these interactions, and the amplitude drop is kept at a pre-set level during scanning. In tapping mode, permanent shearing forces are almost eliminated and the intermittent tip contact with the sample surface occurs at a high frequency (tens and hundreds of kHz) that also restrict material damage. Such operation is gentler than the contact mode, despite the fact that stiffer probes are used in tapping mode. This mode has revolutionized AFM applications because a broad range of samples and materials of industrial importance has become accessible for studies at ambient conditions. For example, the contact mode measurements of Si wafers caused a surface damage that can be avoided by using tapping mode.

The advantages offered by tapping mode for imaging of soft materials are balanced by the complexity of dynamic tip-sample force interactions that in some cases makes the analysis and interpretation of tapping mode images quite challenging. The main problem is that a change of amplitude of an oscillating cantilever while it interacts with a sample does not solely determine tip sample forces. Alterations of the resonant frequency and phase of the cantilever are more sensitive for this purpose. Corrugated surface features as well as contamination traces make the sensitive phase and frequency measurements less applicable for feedback than the amplitude changes. Therefore the amplitude is used for feedback and the vertical adjustments of the piezoscanner needed for keeping the amplitude drop constant are reflected in the height image. The phase changes of the interacting probe during imaging are presented in the phase image, Figure 1b. Usually in the tapping mode, the height and phase images are recorded simultaneously. Phase imaging is most valuable for compositional analysis of heterogeneous samples [16]. Differences in adhesive and mechanical properties of different components are responsible for various phase contrast observed on these samples during imaging. The tapping mode with phase or frequency detection also made possible broad applications of electric force microscopy and magnetic force microscopy.

Qualitative differences of mechanical, adhesive, electric, magnetic and other properties are sufficient for compositional mapping, yet the demand of local quantitative measurements of these properties is increasing with developments of nanoscience and

nanotechnology. The local measurements have been a challenge since the introduction of AFM, and there are a number of relevant problems. They include preparation of specialized probes, optimization of instrumentation, and a lack of appropriate theoretical analysis of the tip-sample forces at the nanometer scale.

At present, tapping mode is the most common AFM mode. In its applications, researchers are always facing a problem in getting the most valuable information, which can be rationally understood. The crucial issue is a correct choice of instrumental parameters for high-resolution surface imaging and compositional mapping of heterogeneous samples, which are usually quite different to achieve these goals. The principal issue of AFM is tip-sample forces and their control. Minimization of the tip-force allows avoiding surface damage and reducing the tip-sample contact area that facilitates high-resolution imaging. Compositional mapping will benefit from an increase of tip-forces because differences between mechanical properties will be better manifested in this case.

High-resolution imaging is the unique feature of STM and AFM. STM observations of atomic defects on semiconductor and metallic surfaces have proved true atomic-scale resolution with this technique. Image resolution in AFM is a complicated issue. In the contact AFM mode, images of crystal surfaces show atomic-scale patterns identical to the crystallographic lattices [13]. The absence of atom-size defects in such images suggests that the tip contact area in this mode is larger than the atomic size. This does not exclude a possibility of lattice imaging based on periodic variations of the normal and lateral forces, which are exercised by a tip when it is moving along a periodical surface [17]. The imaging resolution of tapping mode and of another oscillatory mode—frequency modulation, used for AFM in UHV has different issues. It is clear that contact area of the tip should be comparable with a size of features to be resolved. In general, the contact area is determined by mechanical characteristics of the tip and sample as well as by the apex radius and the tip-force. In UHV conditions of clean sample surface and high quality factor of the oscillating probe, a fine tip-force control is realized by detection of small frequency shifts. Such measurements in frequency modulation mode can be performed with true atomic resolution as confirmed by images of atomic-scale defects [18]. In air, the precise force control is limited, and the best image resolution achieved in tapping mode applications with etched Si probes (apex radius $\sim$10 nm) is around 1 nm. Recent experiments with the sharper probes – carbon spikes grown at the end of a commercial Si probes, have been successful, and true molecular scale resolution was obtained in imaging of surface of polydiacetylene crystal [7]. The tapping mode image of 20 nm on side (Figure 5a) revealed a well-defined pattern with almost vertical rows and a few molecular-size defects of 3–5 angstroms in size. This observation confirms true molecular resolution of the image. Bright spots along the rows are assigned to individual side groups of the polymer chain forming the crystal. In general, the regular molecular order is consistent with the dimensions of the crystallographic surface lattice ($b = 0.491$ nm, $c = 1.410$ nm, $\alpha = 89.5^\circ$, Figure 5b) and with the pattern observed in the contact mode images of the same surface, Figure 5c. The use of the probes with carbon spikes that allow imaging with true molecular resolution requires definite precautions such as a gentle engagement and the low-force operation to avoid a fracture of sharp spikes. Imaging

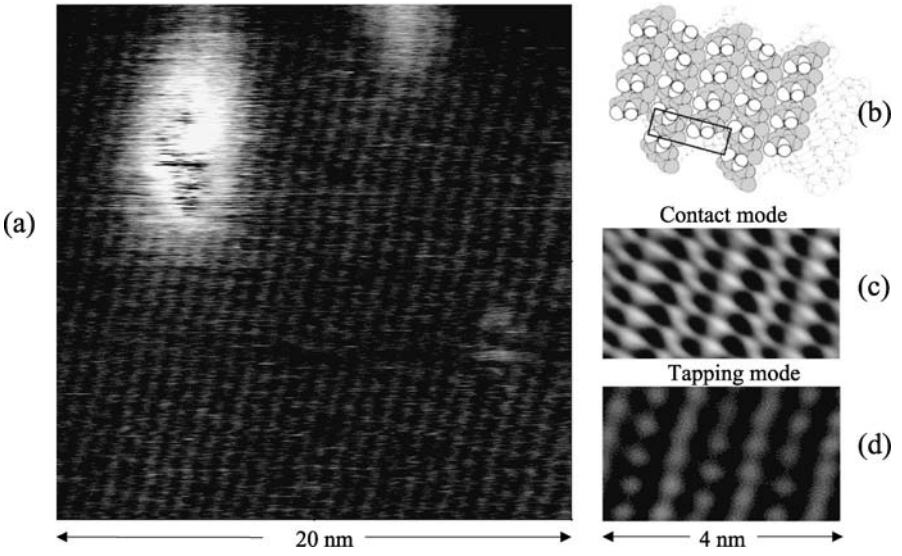

Figure 5. (a) Height AFM images, which were recorded in tapping mode with the novel carbon probe on the *bc*-plane of the polydiacetylene crystal. (b) Molecular arrangement at the *bc*-plane of the crystals of polydiacetylene [2,4-hexadienylenebis(p-fluorobenzenesulfonate)]. Most elevated F, H and C atoms at the *bc*-surface are shown as the unfilled circles and other atoms of the side groups, which are slightly lower, are shown as the gray circles. (c) Contact mode image of the *bc*-plane of the polydiacetylene crystal. (d) Tapping mode image of the *bc*-plane of the polydiacetylene. The 2D FFT filtering (only the most pronounced reflexes of the 2D power spectra were applied for a reconstruction of the surface lattice) led to the periodical patterns in (c) and (d), which were obtained from the images in Ref. S. N. Magonov, G. Bar, H.-J. Cantow, H.-D. Bauer, I. Müller and M. Schwoerer, *Polym. Bull.* 26 (**1991**) 223 and in (a).

of corrugated surfaces with these tips is rather challenging due to possible interference of several spikes, which grow at the same apex.

Two other successful examples of high-resolution imaging with the spikes are shown in Figures 6a–f. In these figures, the images of Si wafer surface and low-K polymer coating [19], which were obtained with these probes, are compared with the images of the same samples recorded with regular etched Si probes. It is obvious that nanoscale roughness of Si surface is much higher in the image obtained with the sharper probe, Figures 6a–b. This is even better seen in the cross-sectional height profiles seen in Figures 6c–d. There are also evident differences of the size of dimples and grains in the images of the nanoporous low K coating. Again the application of the shaper probe provides the height image with much finer surface structure than the use of the regular probe.

An example, which illustrates compositional mapping, is given in Figures 7a–d, where one sees height and phase images of a layer of ultra long alkane $C_{390}H_{782}$, which were obtained at low-force (light tapping) and high-force (hard tapping) imaging. In light tapping, the height image, Figure 7a, shows a number of linear elevations, which

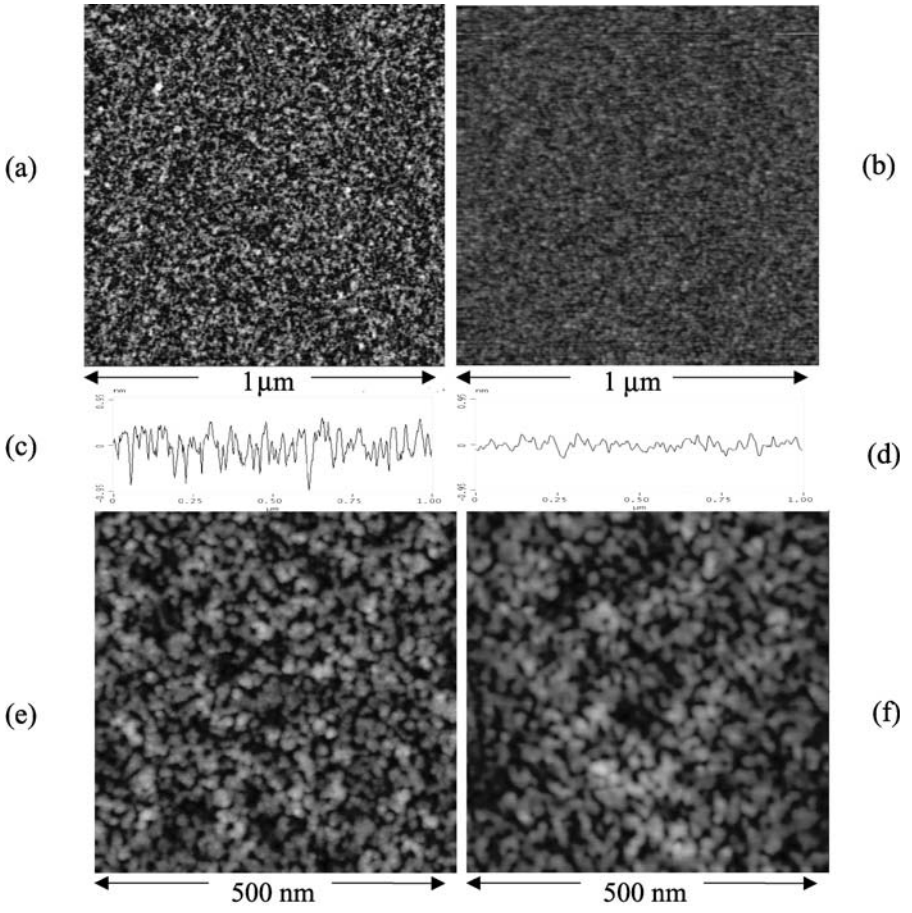

Figure 6. (a)–(b) Height images of Si wafer obtained with the probe with carbon spikes and with regular etched Si probe, respectively. (c)–(d) Cross-section height profiles taken across the images in (a) and (b), respectively. (e)–(f) Height images of a nanoporous low K material obtained with the probe with carbon spikes and with regular etched Si probe, respectively.

are running from left to right. The corresponding phase image (Figure 7b) exhibits only minor contrast at the elevations similar to one expected from the error image. In ideal case of light tapping, the probe should track a samples surface lightly enough that the phase response is not different from the phase of the non-interacting probe. This condition can be achieved when the set-point amplitude, A_{sp}, is close to the amplitude of a non-interacting probe, A_0, in immediate vicinity of the sample surface. The tip-sample force increases with decrease of A_{sp} and hard tapping conditions is usually correspond to $A_{sp} = 0.4–0.5\ A_0$. Height and phase images of the alkane layer in Figures 7c–d, which were recorded at hard tapping, are different from those in

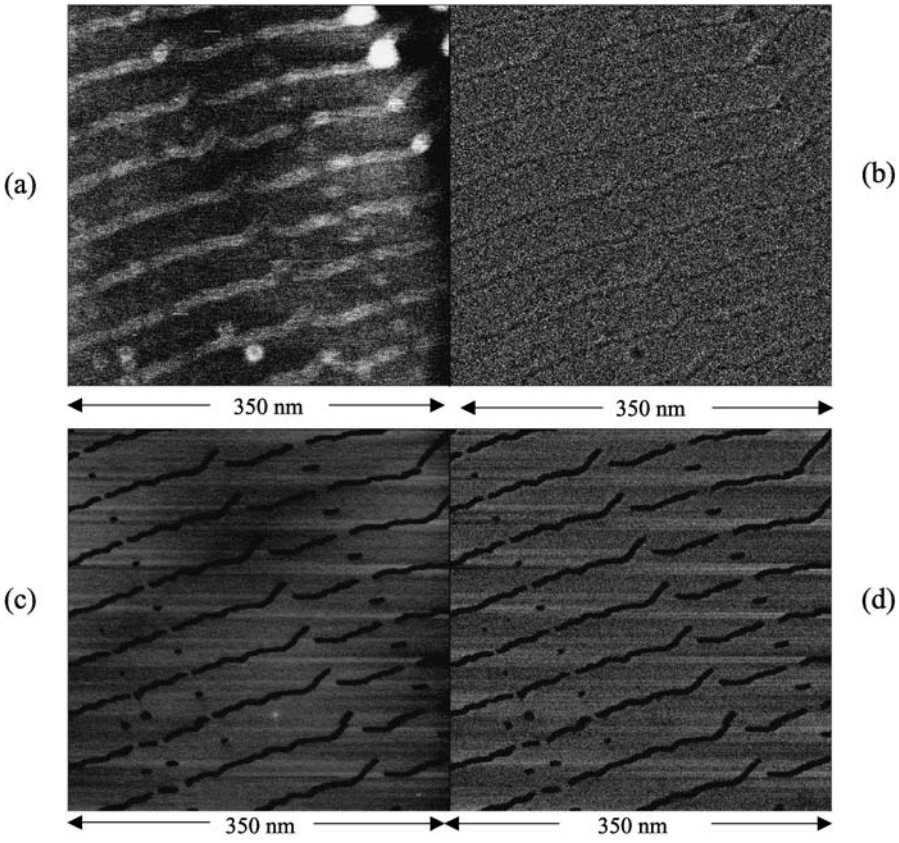

Figure 7. (a)–(b) Height and phase images of ultra long alkane $C_{390}H_{782}$ layer, which were obtained at light tapping. (c)–(d) Height and phase images of the same area as in (a)–(b), which were obtained at hard tapping.

Figures 7a–b, and these changes were reversible. The most pronounced variations are in the contrast of linear features, which are either brighter or darker compared with the rest of the area. The fact that the repeat distance across the stripped pattern (~48 nm) is close to the length of the extended chain of $C_{390}H_{782}$ alkane, suggests that the linear features present the chain ends. On one hand, the end -CH_3 groups of the alkane are more bulky than –CH_2- of the alkane chain and they also are mobile being the chain ends. Therefore, these locations are seen as elevated in height image obtained in light tapping. On other hand, the mobile chain ends do not resist the probe penetration through the alkane layer close to the substrate when hard tapping conditions are applied. This is consistent with the contrast change at these locations from bright to dark in the height image and also with the appeared dark contrast in the phase image. Note that the width of the linear features assigned to the chain ends is

larger than the size of two individual $-CH_3$ groups which come to this interface from the neighboring lamellae. We could not exclude that, in addition to $-CH_3$ groups, a few neighboring $-CH_2-$ groups may contribute to the pattern changing in the AFM images. The finding that the width of the interlamellar interfaces seen in AFM images is increasing as temperature raises supports this suggestion. Molecular dynamic simulations of alkanes on substrates predicted similar effect [20]. The assignment of the dark strips seen in the height and phase images Figures 7c–d to the interlamellar interfaces led to another important result. The dark strips in these images are not always continuous, and one can see one linear dislocation and few locations where short dark strips are shifted a half lamellar size with respect to the main strip. The latter defects are most likely associated with bridging molecules or their blocks in which chains are shifted along their main direction with respect to the other molecules in the same lamellae. These and other defects, which are resolved in AFM of various alkanes at different temperatures will be discussed elsewhere [21]. Here we state that imaging at various tip-forces is useful procedure that provided valuable data about structural organization of alkane layers on graphite.

Our experience shows that on transition from light to hard tapping, the well-defined changes in height and phase images, similar to those seen in Figures 7a–d, are quite rare. Usually, they occur when differences in mechanical properties of surface locations or sample components are large. In many other cases, imaging in hard tapping leads to pronounced contrast variations in phase images whereas height images might change insubstantially. The high sensitivity of the phase images to sample heterogeneities made phase imaging an invaluable constituent of AFM.

A simple protocol can be applied for variable force imaging in the tapping mode. In the beginning of the experiment, the resonant frequency of the probe is determined in immediate vicinity of a sample surface, and the driving frequency is usually chosen at the resonant frequency. By changing the voltage applied to the piezoactuator, an operator chooses A_0, which typically varies in the 1–150 nm range. An engagement of the probe to a sample surface is important procedure especially when very sharp probes such as those with the spikes are applied. A sewing engagement procedure common for MultiMode and Dimension types of microscopes is best suited for the gentle engagement. After this, scanning of the probe over the sample surface can be performed at different A_{sp}, which is typically is in the 0.9–0.2 A_0 range. The magnitude of A_0 also influences the level of the tip-sample force interactions and larger amplitudes provide high-force operation. In some cases, alterations of A_{sp} and A_0 are not sufficient for compositional mapping of heterogeneous samples and one should apply probes with different stiffness to reach this goal. The stiffer probes are needed when a layer of rubbery material covers a sample surface and a tip penetration through this layer is required to reach underlying structures.

Imaging in Various Environments and at Different Temperatures

For over 10 years, AFM measurements have been typically performed at ambient conditions. An exception is the investigation of biological systems, where samples

should be examined in their natural environment, i.e. in water. Obviously by extending AFM studies to different environments and temperatures the value of this technique will increase enormously and we should expect the progress and interesting discoveries in this field in near future.

Contact AFM mode imaging in water has an advantage due to the removal of a surface capillary layer that increases tip-sample forces. Tapping mode operation in liquid faces a substantial lowering of the cantilever resonant frequency and its quality factor. This is evident from a comparison of the amplitude-versus-frequency curves shown in Figures 8a–b. After immersion in water, the resonant frequency of the cantilever with a spring constant of ~0.4 N/m, which we often applied for imaging of polymers under liquid, has dropped more than a factor of two and Q-factor changed from 130 to 4. These effects should be taken into account while imaging in liquids, and related adjustments of imaging parameters e.g. an increase of feedback gains will help avoid an unnecessary tip-force increase.

One can make use of imaging in liquid in different ways. For example, a selective swelling or etching of individual components of heterogeneous materials assists in revealing the microphase separation in such systems. This is especially valuable if the material components have similar mechanical properties that making their recognition in phase images obtained by hard tapping difficult. Such capability is illustrated by the images shown in Figures 8c–d. A microphase pattern in thin film of polystyrene-block-polyvinylpyridine, PS-*b*-PVP, block copolymer, which has been subjected to a long-term annealing at high temperature, is barely seen in the height and phase images recorded at ambient conditions. Immersion of this sample into acidic water (pH = 2.2) is followed by a slow development of bright spheres, which reflect the swelling of PVP blocks. With time, the number of spheres has increased and their hexagonal order becomes evident. These observations confirm the build up of this morphology during temperature-induced microphase separation. Selective swelling combined with *in situ* AFM observations can be also applied visualization of morphology development during crosslinking of rubber materials.

The possibilities of AFM imaging in liquid for industrial research are enormous because they provide access to materials behavior in real life cases. Studies of biomaterials such as implants, contact lenses, drug release systems, etc. will benefit from such applications. Placing a sample in liquid might lead to its excessive softening; therefore, imaging in vapors of different solvents might be a practical and useful alternative. Both studies in vapor and in liquid can be also combined with temperature variations that further expand the range of AFM applications.

AFM measurements at different temperatures have advanced in last 5 years but they still far from routine. The main reason is instrumental difficulties in performing experiments at high and low temperatures. The hurdles associated with temperature control of a sample and of the microscope components surrounding have been only partially solved. The extra functions are usually needed for variable temperature AFM imaging include cooling of the piezoscanner, dual heating of the sample location using sample and probe heaters, monitoring of the surface temperature with 1°C accuracy by using the temperature dependence of the Si probe resonant frequency,

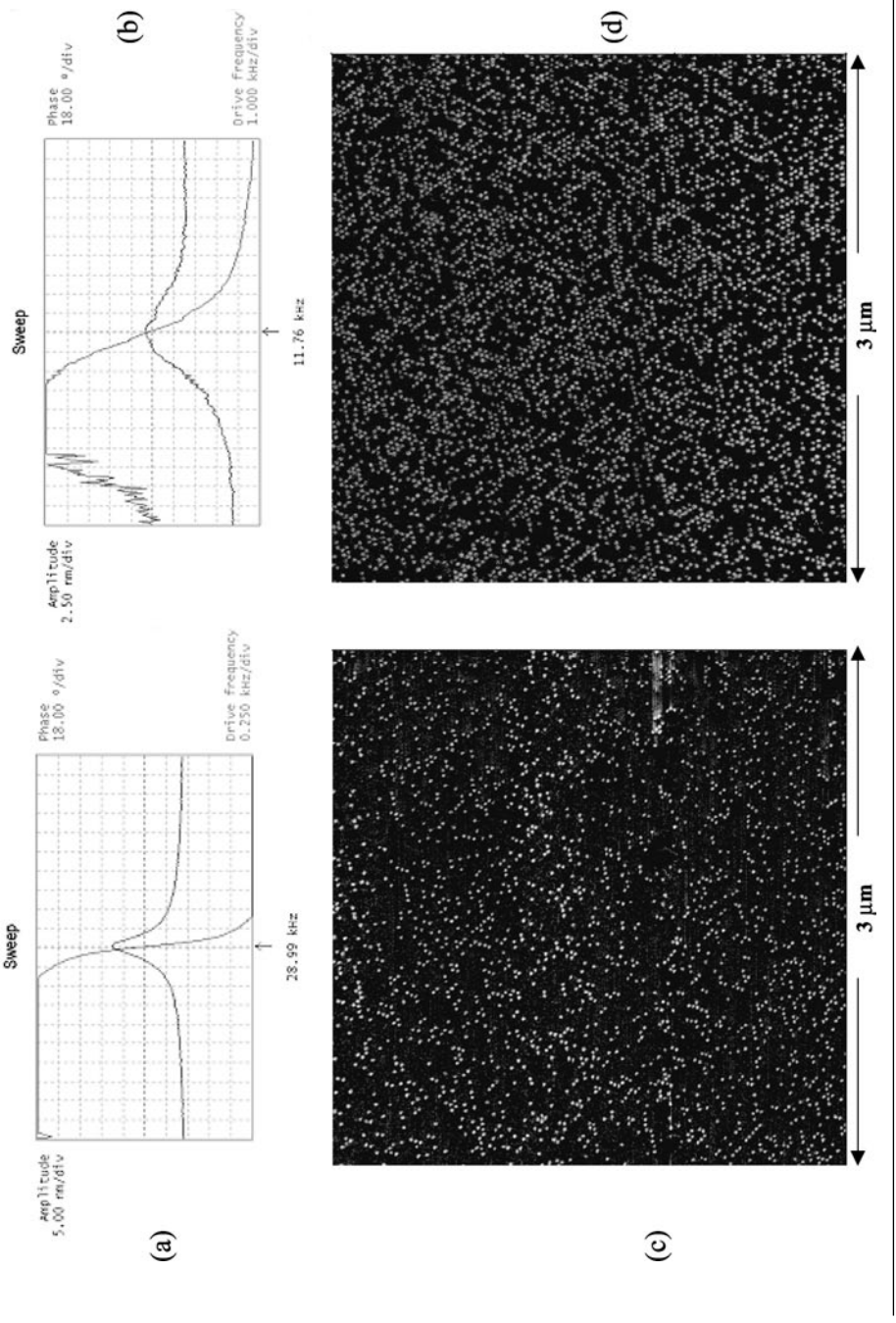

Figure 8. (a)–(b) Amplitude-versus-frequency curves of tapping mode in air and in liquid, respectively. (c)–(d) Height images of polystyrene-block-polyvinylpyridine block copolymer, obtained in acidic water 10 and 40 minutes after immersion.

and environmental control of the sample by purging with inert gases, such N_2, Ar, He [22]. The inert atmosphere is required for high-temperature imaging of some polymer samples to avoid their oxidation. This achieved by purging with He gas, whose presence is easy monitored by increase of the cantilever resonant frequency and quality factor.

At present, researchers are performing AFM experiments at elevated temperatures up to 250°C–300°C and capability of imaging at sub-zero (°C) temperatures is under development. Temperature measurements can be also conducted in vacuum although the AFM studies in vacuum are much less common than those in air. Imaging at elevated temperatures is usually aimed at monitoring structural changes in materials related to different thermal transitions such as melting, crystallization, recrystallization, glass transition, etc. Measurements at elevated temperatures are not much different from those at room temperature yet when approaching melting temperature one might use larger oscillation amplitudes of the probe in order to overcome increasing adhesive tip-sample interactions.

Imaging of polymer samples at elevated temperatures provides some new and unexpected data helping to address important questions concerning polymer structures and their behavior. For example, in the AFM study of structural organization of liquid crystalline carbosilane dendrimers, heating and cooling of thick dendrimer films led to the counterintuitive discoveries of shrinkage and expansion of some ordered domains [22]. This behavior has been explained by anisotropic thermal expansion of these liquid crystalline systems. Visualization of structural changes, which accompany heating of an ultra thin film of low-density polyethylene (PE), has revealed a recrystallization process [23] that was not obvious from differential scanning calorimetry (DSC) data. Spherulitic morphology of the LDPE film had disappeared when the temperature of the sample reaches 80°C and immediately after that large lamellar platelets start to grow. A continued raise of the sample temperature leads to complete melting at 115°C, expected from DSC data. *In situ* AFM monitoring of melt crystallization of poly(ethylene terephthalate), PET, showed that stacking of polymer lamellae governs this process [24]. Visualization of the lamellar stacking is crucial for understanding of the X-ray diffraction studies of this polymer, which require reliable models for a rational interpretation of the reciprocal space data. AFM observations of morphology of semicrystalline polymers and, particularly, their nanometer-scale granular structure, which was found on polymer surfaces and in bulk, were among the factors that revitalized strong interest in the studies of polymer crystallization. Two examples of visualization of the grain structure of polymer surfaces are presented in Figures 9a–e. The images of syndiotactic polystyrene at 170°C and 240°C are shown in Figures 9a–b. The lamellar morphology, which is distinctively seen in the first image, characterizes the β-phase of this polymer. At temperatures close to the melting point, grainy structures appeared as is evident from the second image. Similar changes from lamellar to grainy morphology were also observed in samples of melt-crystallized PET, shown in Figures 9c–e. This transformation had occurred when the sample temperature was lowered below Tg of this polymer. These observations suggest that granular morphology could arise either due to a disintegration of polymer lamellae into smaller blocks near its melting or from a solidification of the amorphous material surrounding

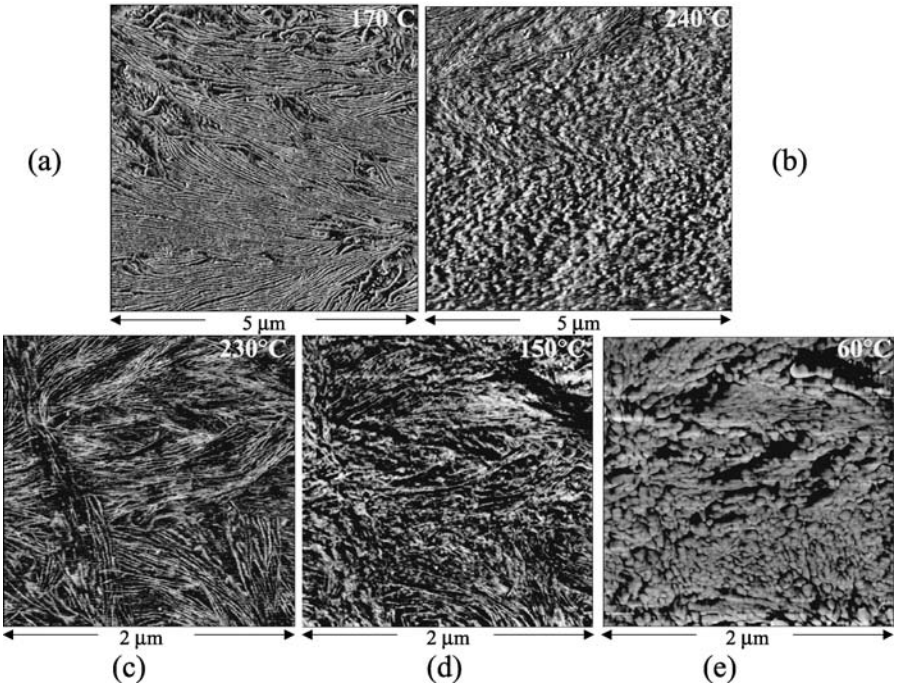

Figure 9. (a)–(b) Phase images of β-syndiotactic polystyrene obtained at 170°C and 240°C, respectively. (c)–(e) Phase images of melt-crystallized PET at 230°C, 150°C and 60°C, respectively.

the lamellar core. In the second case, an AFM probe penetrates through the top-most amorphous material when it is in rubbery state and reaches the ordered lamellar core.

To date, AFM studies at low temperatures are less common than those at elevated temperatures. Crystallization of polydiethylsiloxane from mesomorphic phase proceeds at temperatures around 0°C and it is accompanied by morphological changes shown in Figures 10a–c [25]. An array of mesomorphic lamellar aggregates, which is seen in Figure 10a, underwent gradual crystallization as the temperature of the samples was dropped to –5°C and kept at this level. The crystallized material is characterized by lamellae with sharper edges, which also exhibit a brighter contrast in the phase images. Phase images (Figures 10b–c) demonstrate that the crystallization front has moved from the top to the bottom of the scanning area.

There is another expectation, which is related with AFM studies at low temperature. Small objects such as single macromolecules deposited on different substrates can be seen in AFM images only if they adhere to the surface strongly enough to resist the tip-force they experience during imaging. This statement has been confirmed by the finding that single polymer chains, which are observed at room temperature, are not seen in AFM images at elevated temperatures. They are most likely detached from

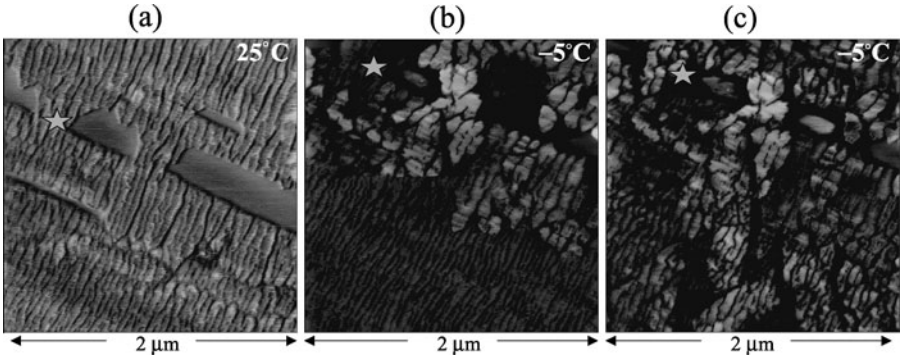

Figure 10a–c. Phase images of polydiethylsiloxane, which were taken at room temperature (a) and after cooling to −5°C (b)–(c).

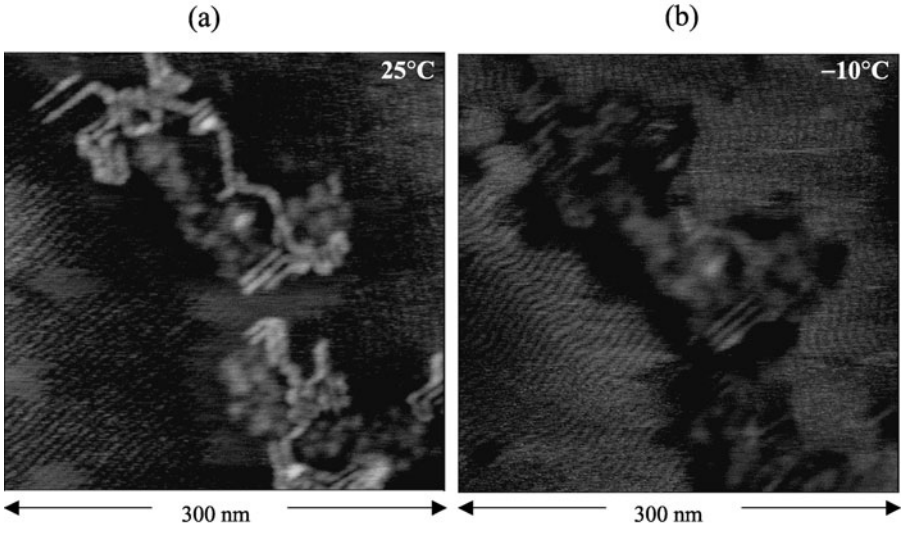

Figure 11. (a)–(b) High-resolution height images of single chains of polyphenyleneacetylene with mini-dendritic groups at 25°C and at −10°C, respectively.

the substrate due to their increased mobility. The molecules return to the substrate when the sample temperature is lowered back to room temperature. Consequently, at room temperature we might also see only part of the surface material deposited on a substrate. Therefore, observations at low temperatures can assist us in visualizing more surface species not seen at room temperature. With this in mind, we performed imaging of polymer chain molecules with mini-dendritic groups, and some of the results are shown in Figures 11a–b. Figure 11a shows an aggregate of several macromolecules,

some of which exhibit straight segments, grains, which are surrounded by periodical structures. The latter structures are not rare but not well-understood guests in images of single polymer macromolecules deposited on different substrates from very dilute solutions. The second image (Figure 11b) obtained at the sub-zero temperature, shows differences in the shape of the macromolecules most likely related to conformational rearrangements induced by the temperature decline. Although in this case, we noticed only alterations of the molecules seen at room temperature, forthcoming studies will help us observe additional surface species.

Researchers, who are regularly using AFM, are aware of different factors that affect image reproducibility. Not only is calibration of piezoscanners and checking tip sharpness necessary, additional steps are needed to improve image quality. Specific topographic features and surface roughness can cause undesirable image distortion. Sharpness and symmetry of the tip apex are the main source of image distortion when surfaces have features comparable in size and shape with the probe extremities. Therefore, use of several different probes might help avoid misinterpretation. Probe shape changes might happen during scanning either as the result of a mechanical damage of a tip shape during imaging of a hard surface or due to tip contamination by surface material if a sample is sticky. Operation at low forces is useful to get away from the first problem and might also help avoid the second.

Studies of homogeneous surfaces are less subject to image variations compared to studies of heterogeneous surfaces with locations of different stiffness and adhesion. In addition to the image variations caused by geometric factors, alterations of images of heterogeneous materials are also related to different responses of individual components to the tip-force. Therefore, some images changes could be related to force variations. Images with a pronounced contrast of individual components are usually obtained in operation imaging with elevated forces. For rational imaging of heterogeneous materials, a researcher should find a set of experimental parameters (A_{sp}, A_0, the probe stiffness, etc) most suitable for compositional mapping of a particular family of materials. In this respect it useful to examine model samples which are prepared by varying a composition of a particular blend or multicomponent material.

IMAGING OF MACROMOLECULES AND THEIR SELF-ASSEMBLIES

Visualization of Single Polymer Chains

AFM provides the unique capability to visualize single macromolecules and their size, conformation, surface interactions and other phenomena can be studied by analysis of the image. Preparation of samples for such observations is straightforward; the only challenge being fixation of individual molecules to the surface. AFM images of DNA are the best known and three are presented in Figures 12a–c. The large-scale image shows numerous DNA strands spread on a mica substrate. A close look at a few of them in the height images, which were obtained in light and hard tapping, revealed variations of the shape and width of the curved structures representing the macromolecules, Figures 12b–c. These changes are reversible and can be assigned tentatively

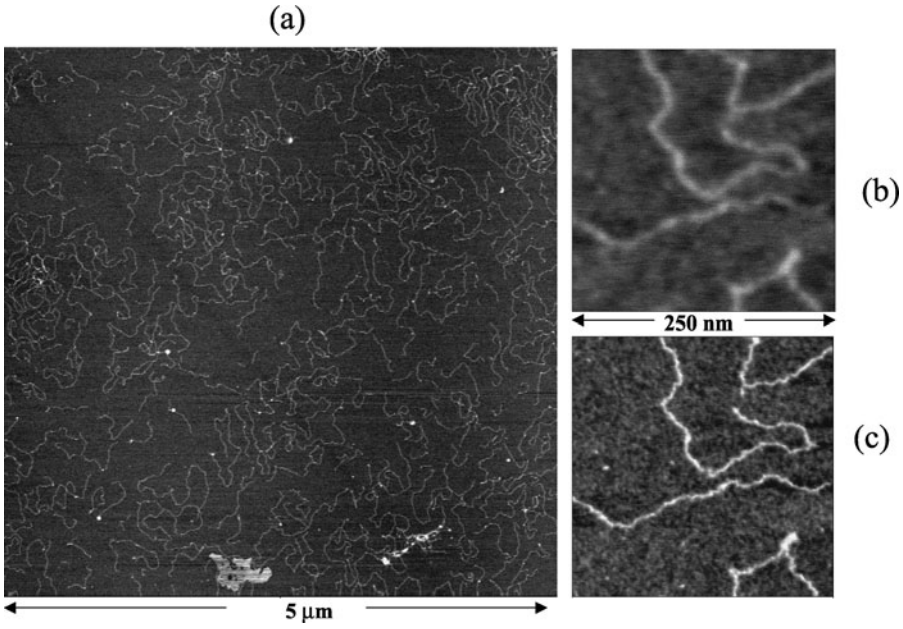

Figure 12. Height images of DNA molecules on mica, which were recorded in air. The images in (a) and (b) were obtained in light tapping, the image in (c) – in hard tapping.

to a soft "jacket" existing around the DNA core on mica, which can be depressed by the tip.

Since the first AFM studies of nano-scale objects, which also include single polymer macromolecules lying on substrates [26, 27], one of basic questions is how relevant is their height and width measured in the images compared to their real dimensions. One can foresee at least two reasons why AFM images of single macromolecules on surfaces might give the dimensions different from those in bulk or in solution, which are measured by other methods. The first reason is related to a possible relaxation of macromolecules on substrates that lead, for example, to their flattened shape. The second reason is due to peculiarities of AFM. Convolution of the tip-shape with real macromolecule dimensions is responsible for their widening in the AFM images. Also, one should not exclude tip-force induced deformation of the macromolecules that causes a height reduction. In contrast to the macromolecules' width, a contour length of extended macromolecules can be measured more precisely. For a number of polymers, whose chain molecules adopt an extended conformation on a substrate, the contour length can be considered as a measure of its molecular weight. The histograms, which reflect a distribution of contour length for large number of single macromolecules as measured from AFM images, have been compared with molecular weight distribution estimated from GPC and light scattering data [28].

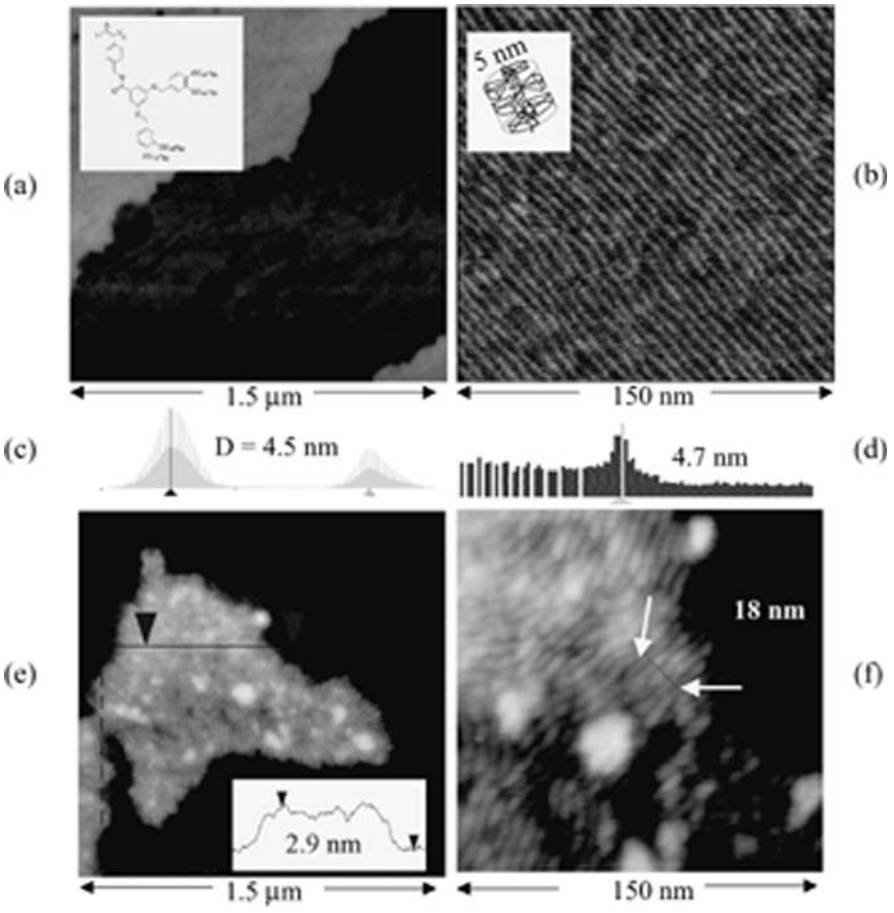

Figure 13. Height image (a) and phase image (b) of a sample of polyphenylacetylene with mini-dendritic groups representing the molecular order in bulk. The inserts in top left corner of these images show a chemical structure of the polymer and a sketch of the polymer conformation in bulk estimated from the X-ray data, respectively. The height histogram in (c) shows an average thickness of the top layer in (a). The power spectral density plot in (d) reveals the spacing of the molecular order in (b). Height and phase Images of the same polymer deposited on mica from dilute solution are shown in (e) – height image and in (f) – phase image. The insert at the bottom of the image in (e) shows a height profile across the polymer domain in the direction indicated with the arrows. The arrows in the image in (f) define the combined width of 4 polymer chains, which equals to 18 nm.

Issues related to size of polymer macromolecules in bulk and on surfaces as well as possible tip-force induced deformation have been explored in study of polyphenylacetylene with mini-dendritic groups. To prepare the sample surface, a polymer layer in melt was squeezed between two flat substrates and cooled. This sandwich was then split through the ordered material and examined with AFM. The image in Figure 13a shows a layered structure of this material in bulk. A regular packing of

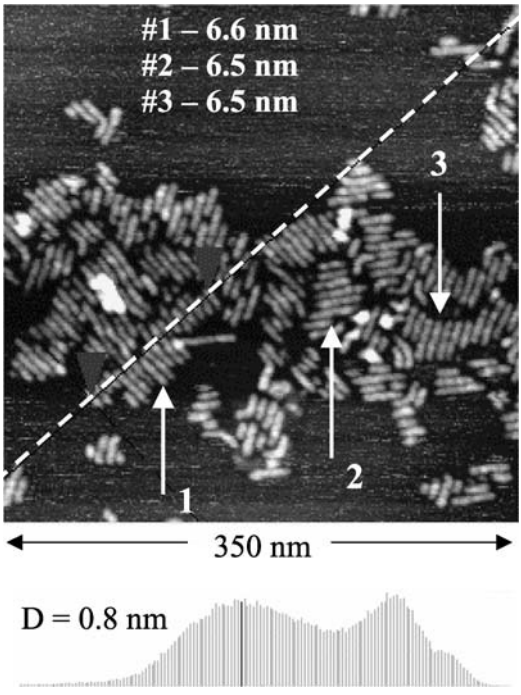

Figure 14. Height image of an aggregate of single chains of polyphenylacetylene with mini-dendritic groups, which were deposited on graphite from dilute solution. The number at the top of the image show the average width of the chains in the stacks indicated with the arrows.

extended linear structures is seen in the high-resolution image in Figure 13b. The power spectral density plot, which is presented below this image, revealed 4.7 nm spacing between these structures. This dimension is close to the 5-nm size of individual polymer chains in the hexagonal columnar arrangement of these molecules in bulk as revealed by X-ray analysis.

The chain molecules of the same polymer were observed on mica and graphite in samples prepared by spin casting of the dilute polymer solution. A domain of the macromolecules on mica is shown in Figure 13c. Its height, 2.9 nm, is slightly less than one expected based on the size of the individual polymer chains. A high-magnification image, Figure 13d, shows that the domain is formed of linear features whose estimated width is ~4.5 nm. Therefore, the size of the polymer chains on mica is close to their size in bulk. A partially reduced height of the chains on mica might be due to slight height depression by the tip. Estimates of the polymer chain dimensions on graphite from the AFM image in Figure 14 indicate that the macromolecules' height is much smaller and their width is larger than those of the chains on mica. This finding suggests substantial spreading of the single polymers on graphite.

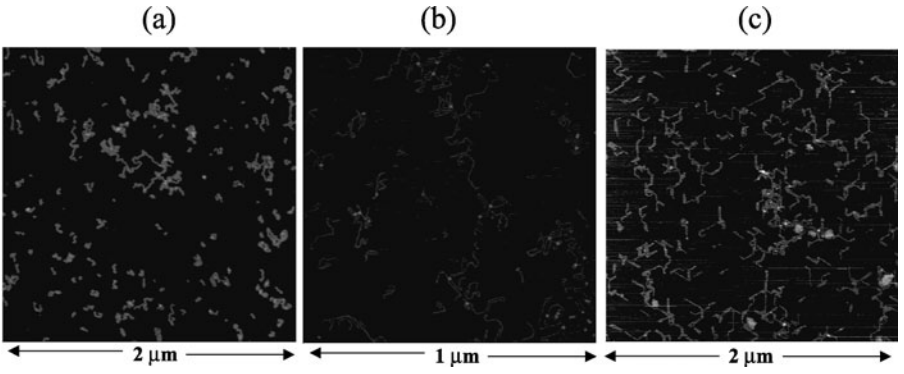

Figure 15. (a)–(c) Height images of single macromolecules of polymethylmethacrylate with mini-dendritic groups, which were deposited on mica, graphite and WSe_2, respectively.

Remarkably, the macromolecules on graphite are seen in the shape of individual straight or bent rods whose orientation reflects their epitaxy on the substrate. As a result of this epitaxy, the molecules are unraveled along surface lattice directions of the graphite. This phenomenon is common for alkanes and polyethylene, and the fact that the 0.25 nm spacing of the graphite lattice. The repeat distance along the alkyl chain in all-trans conformation is close to 0.25 nm, and this is believed to be the reason for the epitaxy. The multiple examples show that a presence of alkyls at the terminals of mini-dendritic side group of polymers also leads to the same arrangement [29]. Single macromolecules of polymethylmethacrylate (PMMA) with mini-dendritic groups, which were deposited on mica, graphite and WSe_2, are shown in Figures 15a–c. WSe_2 is the inorganic layered material with an atomically flat surface made of Se atoms in the closed hexagonal packing with the inter-atomic distance of 0.32 nm. Mica is also an atomically flat substrate, the surface atoms of which are arranged in a hexagonal order with an inter-atomic spacing of 0.52 nm. The arrangement of the chains on WSe_2 is similar to graphite, whereas on mica, the individual macromolecules are less extended and do not epitaxially orient on the substrate. This finding suggests that the epitaxy on graphite and WSe_2 is governed more by the overall symmetry than by the matching of the atomic-scale spacings of the substrate. The hydrophilic nature of mica has imposes restrictions on the unfolding of these macromolecules.

Height-temperature AFM measurements of PMMA chains with mini-dendritic groups on the above mentioned substrates as well as the experiments on the tip-force assisted transport of these objects on the substrates help understanding the individual macromolecules' adhesion [30]. Thermal motion of the unfolded chains was observed on graphite and WSe_2 as soon as the sample temperature was raised 10–20 degrees above room temperature. With further temperature increase, the macromolecules were not seen in the images because their adhesion to the substrate was too poor to resist a tip-force. Mostly likely, the chains were floating in the liquid contamination layer, which present on surfaces in air. The situation was quite different on mica,

where the chains and their aggregates were observed without any positional changes even at temperatures above 200°C when partial thermal degradation has started. Strong adhesion of these polymer chains to mica is confirmed by the unsuccessful attempts to move the macromolecules across the substrate. These attempts led to cutting of the chains into pieces [30]. The tip-assisted transfer of the same macromolecules on graphite and WSe_2 was successful, and the macromolecules have been moved along the tip trajectories.

Alkanes, Polyethylene and Fluoroalkanes

To demonstrate the capabilities of AFM for studies of self-assembly and order in ultra thin layers we will consider several results obtained on alkanes of different length and single crystals of polyethylene (PE), one of the most important industrial polymers. When alkanes are deposited on graphite by spin casting of their diluted solutions, they form layers with the well-defined epitaxial order as shown in the images of $C_{36}H_{74}$, Figures 16a–b. The domains with differently oriented striped structures are seen in the larger-scale image. The other image shows the alternating bright and dark strips whose order is characterized by a spacing of 4.7 nm corresponding to the length of the extended alkane molecule. By analogy to the layers of $C_{390}H_{782}$, the darker regions can be assigned to the interlamellar interfaces where mobile $-CH_3$ groups and few their $-CH_2-$ neighbors are located. With the increase of a concentration of alkane solution, nanocrystals were formed on the top of the layers as it was observed in study of the alkanes with longer chain, $C_{60}H_{122}$ [31]. In the $C_{60}H_{122}$ samples, the nanocrystals melted around 95°C, while the epitaxial layers were observed at temperatures up to 140°C. In the measurements above the bulk melting point T_m of alkane crystals ($T_m = 95°C$ for $C_{60}H_{122}$), an AFM probe penetrates through a melt polymer and reaches an ordered layer lying immediately on graphite. The lamellar order of this layer, which exhibits an additional thermal stability due to specific interactions with the substrate, has been observed at temperatures up to 50 degrees above T_m. This has been found for $C_{60}H_{122}$, $C_{122}H_{246}$, $C_{242}H_{486}$ and $C_{390}H_{782}$ [21, 32]. The high-temperature images of $C_{390}H_{782}$ layer in Figures 16c–d demonstrate its lamellar order at two different locations. The image at 100°C, which is the temperature below T_m ($T_m = 128°C$ for $C_{390}H_{782}$), shows multiple defects reflecting a relative shift of the chain molecules along its main direction. The lateral extent of these defects is different at various locations, and they heal as the sample temperature approaches 130°C. At the left part of the image in Figure 16c, the remnants of the second layer are seen as single bright strips of the lamellar width. They also disappeared after heating to 130°C. The morphology of the $C_{390}H_{782}$ layer at 140°C, Figure 16d, has distinctive differences compared to the previous one. First of all, the T-type defects, in which two lamellae are merged into one, are the only defects seen at 140°C. Second, a width of brighter strips became smaller than that of the darker strips. This suggests that larger parts of the macromolecules are mobile as temperature was raised from 100°C to 140°C.

PE molecules are essentially extra long alkanes but the main difference is that polymerization leads to variations of the chain length of individual molecules that influence

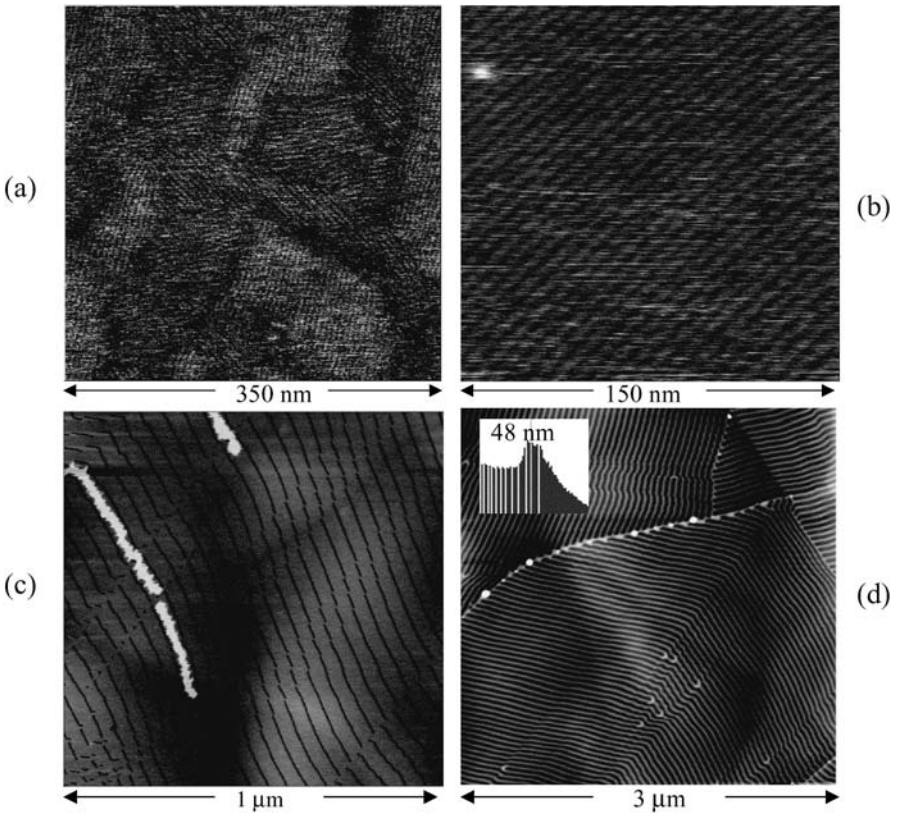

Figure 16. Height images of the layers of $C_{36}H_{74}$ alkane (a)–(b) and ultra long alkane $C_{390}H_{782}$ (c)–(d). Images in (a)–(b) were obtained at room temperature and images in (c) and (d) at 100°C and 140°C, respectively. The insert at the left top corner of the image in (d) shows the power spectral density plot with a value of most pronounced peak.

many properties of these materials. Ultra long alkanes due to their monodisperse nature are the best know models of PE, and these alkanes have been intensively examined during last 20 years [33]. The common feature of ultra long alkanes (starting with alkane with carbon atoms above 150) and PE is that their crystallization in dilute solutions proceeds by multiple folding of individual chains into thin lamellae folded chain structures which have the lozenge shape. The chain folding is the kinetically driven process, and thermal annealing of these crystals promotes a partial unfolding of polymer chains toward the more energetically favorable extended chain conformation. Morphology changes accompanying annealing of single crystals of PE have been of interest for many years [34]. Recent AFM studies of the annealing-induced structural transformations have revealed new details concerning these pathways, which depend on a sample preparation history and nature of the substrate.

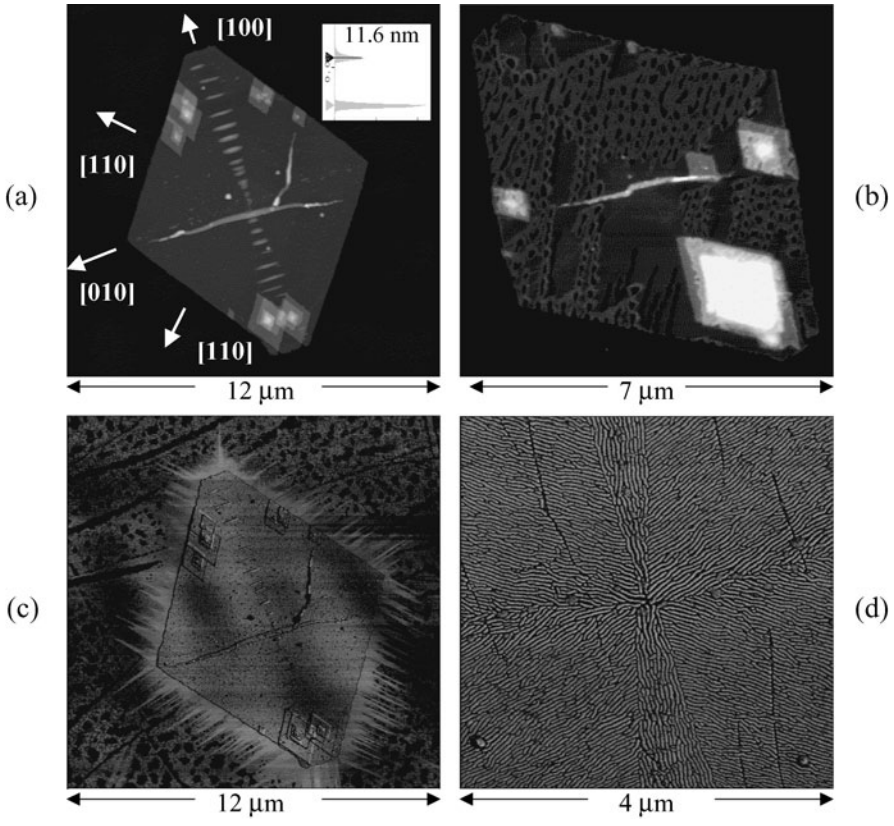

Figure 17. (a)–(b) Height images of dried single crystal of PE on Si substrate before and after annealing at 115°C, respectively. The height histogram in the top right corner in (a) define the crystal thickness. In (a), white arrows indicate different crystallographic directions. (c)–(d) Phase images of wet single crystal of PE on graphite after annealing at 75°C and 140°C, respectively.

Main structural changes, which are observed during annealing of single crystals of PE, are shown in Figures 17a–d. The crystals, which are grown in dilute solution, have a tent-like shape. After deposition on a flat substrate, such crystals collapse and adopt a shape of flat lozenge. A slightly truncated lozenge of PE crystal with a number of spiral overgrowths and a central pleat aligned in the [010] direction is shown in Figure 17a. The polymer chains are oriented in the [001] direction, i.e. almost perpendicular to a substrate. The crystal thickness (11.6 nm) corresponds to the chain stem length, and the top and bottom surfaces are formed of the chain folds. Several tiny wrinkles oriented along the [010] direction define two small (100) sectors and a slightly truncated shape of the crystal. It was found that during annealing of the PE crystals on Si and mica substrates, which were dried under vacuum before the annealing, the polymer chains

unfold without a chain reorientation. This leads to a local thickening and development of the holes, Figure 17b.

Annealing of wet PE crystals (which were stored in air but not dried under vacuum) on the same substrates initiated a formation of lamellar ribbons (edge-on lamellae) in which the polymer chains reoriented parallel to the lamellar surface. The same transformation was found for single crystals of PE on graphite independent from the sample preparation history, Figures 17c–d [35]. In addition, the annealing of the crystals on graphite was accompanied by a substantial outflow of the polymer material from the crystal to the substrate. The image of the crystal after annealing at 75°C shows the outflow of the polymer in the [110] and [100] directions, Figure 17c. The outflow material most likely consists of mobile polymer chains, which were not properly incorporated into the crystal. Annealing at temperatures below 100°C was not accompanied by noticeable changes of the lozenge. The major evolution has initiated above 100°C, and it led to the formation of lamellar ribbons. The ribbons oriented along the [110] and [100] directions completely filled out the crystal sectors of the lozenge, Figure 17d. *In situ* monitoring of the initial steps of this transformation allowed us to suggest that the PE recrystallization and chain reorientation are facilitated by traces of solvent trapped underneath these objects during their collapse on a flat substrate. Analogous chain unfolding pathways were found for single crystals of $C_{390}H_{782}$ [32].

The structural transformations of the single crystals of PE, which are discussed above, were observed during their step-like annealing at different temperatures. When heating of the crystal deposited on mica to 140°C proceeded fast, it caused a complete melting of the crystal as seen by a formation of a large droplet of melt, Figure 18a–b. Quenching of this material to room temperature has been accompanied by recrystallization. The patch of recrystallized material, which remained within the frame of the initial lozenge, is illustrated by the height and phase images in Figures 18c–d, respectively. High-magnification images revealed its fibrilar and granular structures, Figures 18e–f. The fibrilar structures represent the edge-on lamellae whereas the isolated grainy structures can be assigned to the predominantly amorphous material, Figure 18e. The surface of the recrystallized material exhibits grainy morphology similar to one, which was observed on the surface of melt-crystallized low-density PE [36]. AFM investigations of the crystallization and melting processes in a droplet of semicrystalline polymer with known amount of the polymer might be a good model system to study these processes in the confined geometry.

Fluorinated materials have a number of important properties such as low surface energy that ensure their technological value. Semifluorinated alkanes with the structure $F(CF_2)_m-(CH_2)_nH$, F_mH_n, are forming micelles in solution and monolayers at the air-water interfaces [37]. Structural organization of these materials has been examined for a while yet many issues remain controversial. We have applied AFM to study self-assembly of perfluoroalkyl alkane, F14H20, and several results, which illustrate specifics of structural organization of this material, are presented below. In the extended conformation, the fluorinated part of the F14H20 due to large size of F atoms and related steric hindrance adopts a helical conformation with 1.64 nm in length and the

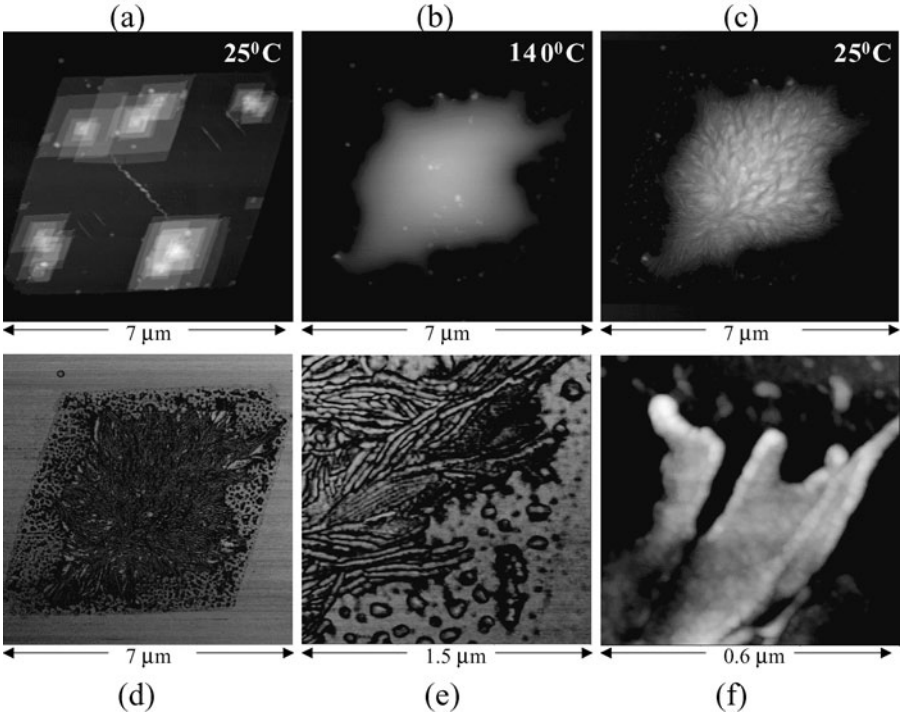

Figure 18. Height images of single crystal of PE on Si substrate at room temperature—(a), after fast heating to 140°C – (b) and after cooling to room temperature – (c). Phase images in (d)–(e) and height image in (f) show structural details of the semicrystalline PE patch formed after cooling from 140°C to room temperature.

hydrogenated part is characterized by the all-trans zigzag conformation with 2.55 nm in length. A width of these parts is also different: 0.60 nm for $-CF_2-$ sequences and 0.48 nm for $-CH_2-$ sequences. In earlier work, monodisperse surface micelles of F8H16, which were transferred from the water subface of Langmuir trough on Si substrate, were observed in AFM images [38]. The micelles have a round shape with a diameter of 30 nm and height of 2 nm in height. A hole in the center makes them look like donuts. These nanoscale 2D objects decorated the substrate being packed almost hexagonally.

When the F14H20 films were prepared by spin casting from dilute solution on different substrates, including a water subface in Langmuir trough, we have observed several types of structures, which depend on solvent and substrate nature. When the material was deposited on graphite from hydrogenated solvents such as decalin and octane, the extended ribbons of 30 nm in width and ~2 nm in height have been seen in AFM images, Figures 19a–b. The ribbons are aligned along three main directions of the substrate that assumes their epitaxial arrangement. Besides these ribbons, several

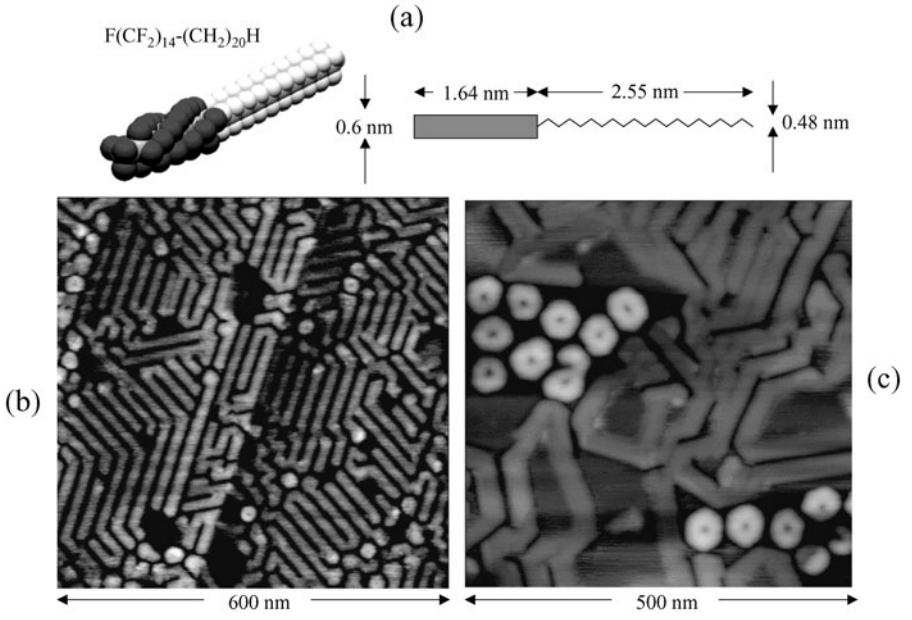

Figure 19. (a) Sketch of semifluorinated alkane F14H20 and its molecular dimensions in fully extended conformation. (b)–(c) Height images of F14H20 nanostructures deposited on graphite from decalin and octane, respectively.

donut-like clusters are seen. In general, the donuts are twice higher than the ribbons. Some of the donuts have a defective structure with a missing quarter of the donut, as seen in the left bottom of Figure 19b. This observation, as well as the fact that the external contour of many donuts exhibits a hexagonal contour, hints that the donuts and ribbons are formed of similar molecular assemblies. Clusters of different shape were formed in fluorinated solvents and deposited on water, mica and graphite as seen from AFM images in Figures 20a–c. Most likely, the circular twisting of the ribbons formed these monodisperse structures with an average diameter of 80 nm, Figure 20a. On mica surface, these clusters were packed in a hexagonal order. The power spectra of 2D FFT, which is shown in the insert in the right top corner of the image in Figure 20a, exhibit two sets of the hexagonal patterns corresponding to the cluster order and to the cluster shape. The clusters on graphite are quite alike yet they exhibit the more pronounced hexagonal shape in Figure 20b as compared to the clusters on mica. There are distinctive differences of the nanoscale morphology of the adsorbates, which were deposited from the hot and cold solutions on graphite. The clusters cast from the cold solution exhibit a fine substructure consisting of sets of linear strips with a 7 nm spacing. Akin linear strips are seen at the substrate locations in between the clusters, which were put on graphite from the hot solution. In both cases, linear structures are oriented in correspondence to the substrate symmetry.

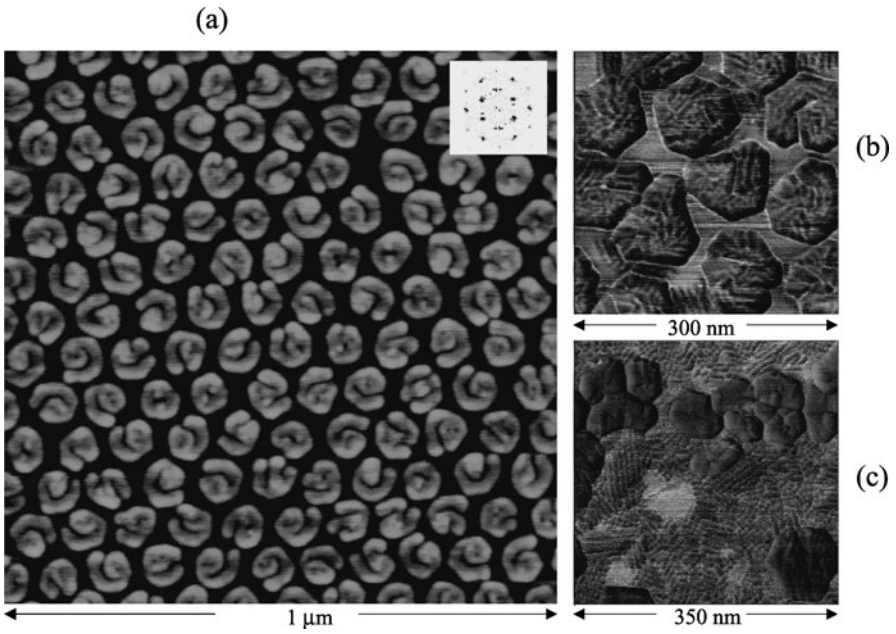

Figure 20. (a) Height image of F14H20 nanostructures deposited on mica from hexafluoroxylene. The insert in the right top corner shows the 2D FFT power spectral density pattern. (b)–(c) Phase images of F14H20 nanostructures deposited on graphite from cold and hot hexafluoroxylene, respectively.

The F14C20 adsorbates, which were deposited on graphite from octane, were examined at temperatures close and above their isotropization temperature of 95°C, Figures 21a–b. In the image recorded at 80°C, the domains with the linear strips similar to those seen in Figure 20c occupy most of the surface area. There are few straight ribbons, which did not melt yet. At higher temperature, the ribbons disappeared, and the domains have transformed into a continuous layer. As in the case of alkane layers on graphite, the F14H20 layer retains its order at temperatures above T_m. The molecular order of this layer is characterized by two spacings: 7.2 nm and 9 nm. The first one describes the linear strips, whereas the second one – the micellar arrangement, which is distinctively seen at the right edge of the image in Figure 21b.

AFM studies of the F14H20 adsorbates provide new information concerning the molecular order in these systems. The fact that the molecular arrangement on graphite shows a hexagonal symmetry implies that alkyl groups are interacting with the substrate. The spacing of the molecular order (~7 nm) is smaller that the double length of the F14H20 molecule. This suggests that either the molecules are tilted within these structures or there is a partial interdigitation of the molecules forming double layer.

AFM provides several important findings concerning self-assemblies of the semifluorinated alkane although these data alone are not enough for complete understanding

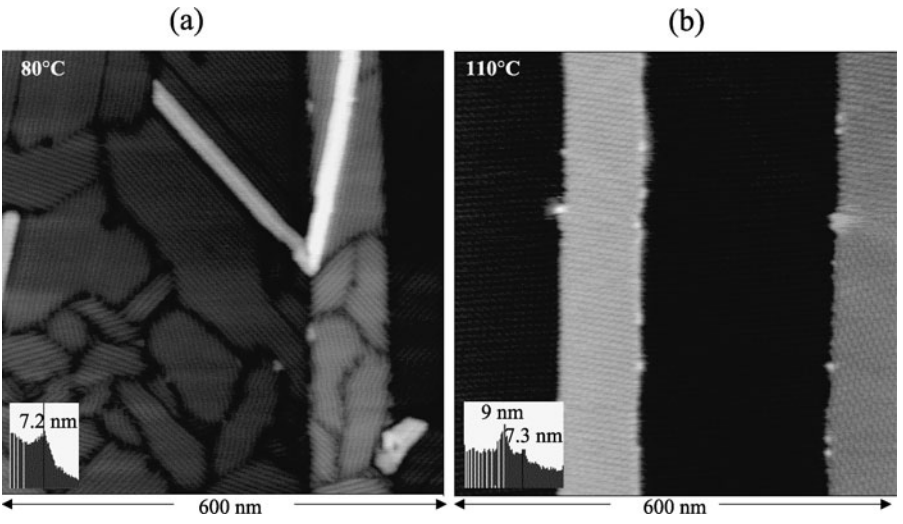

Figure 21. (a)–(b) Height images of F14H20 nanostructures deposited on graphite from octane solution, which were obtained at 80°C and 110°C, respectively. The inserts in the left bottom corner show 2D power spectral density plot and values of the most pronounced peaks.

of their molecular organization. Further interplay of AFM, X-ray diffraction and spectroscopic measurements is needed for accomplish this goal.

STUDIES OF HETEROGENEOUS SYSTEMS

Semicrystalline Polymers

In the following, we will consider AFM studies of heterogeneous polymer systems, which are the most common objects of industrial research. Multicomponent polymer systems present an important class of commercial materials that addresses variety of practical applications. The way these materials are prepared substantially influences their technological properties. Therefore, examination of morphology and composition of multicomponent polymer systems provides key evidence for optimization of their formulation and properties. Strictly saying, heterogeneous materials are those, which consist of components with different chemical components: copolymers, polymer blends, composites, etc., semicrystalline materials can be also assigned to such materials.

In electron microscopy, visualization of lamellar structures of semicrystalline polymers is usually performed on samples, which were etched or stained. These procedures are not necessary for AFM studies because the crystalline and amorphous components are differentiated due to differences of their mechanical properties that are reflected in the probe response. Practically, compositional mapping is achieved with hard tapping when the images demonstrate the distribution of individual components on the sample surface. For many polymer systems, especially those with rubbery-like components, imaging at elevated forces might result in the AFM probe penetration through top

rubbery layer. In this way, more rigid subsurface structures can be seen in the images at the depths up to hundreds of nanometers.

Bulk morphology of polymer samples can be of primary interest and the application of an ultramicrotome is needed to access the bulk polymer structure with AFM. This preparation tool became the important accessory for AFM analysis of heterogeneous polymer samples. It is worth noting that polymer blocks with a smoothly cut surface, which is best prepared with a diamond knife, are usually employed for AFM imaging. Thus an elaborate and time-consuming preparation of ultrathin slices of polymer material, which is required for TEM, is eliminated. It is worth noting that quantitative estimates of the sample composition, in the analysis of AFM images, are more accurately reflect this important characteristics than the data obtained with TEM. The reason is that TEM micrographs present 2D view of a thin but still 3D material section.

First two examples are dealing with morphology of PE films. AFM images of industrial linear low-density PE film, whose surface and near-surface morphology can be examined without any sample preparation, are shown in Figures 22a–b. The height image presents the large-scale surface morphology with corrugated structures formed by micron-size bumps. At higher magnification, lamellar structures are resolved in the phase image. The lamellar edges are seen as individual bright strips or as their clusters at locations where lamellar stacks are present. In addition to the image contrast, individual components of heterogeneous materials can be also identified due to their specific shape. The corresponding example is presented in AFM images of commercial low-density PE, Figures 22c–d. The large-scale surface morphology of this material is different from that in Figure 22a. An orientation pattern is recognized by surface features, which extend from the top left corner to the right bottom corner in Figure 22c.This is a consequence of mechanical stresses during manufacturing of the film. The platelets of a mineral filler are clear seen in the phase image in Figure 22d. Such fillers are added to polymers in order to modify their properties, e.g. adhesion, mechanical strength, flammability, etc.

Block Copolymers

Block copolymers are important components of engineering plastics. In recent years, the interest to these materials is growing because of unique capabilities of tuning their nanoscale architecture through microphase separation. Among new applications areas are nanolithography and the templating of inorganic structures such as nanowires and magnetic dots. Extended ordered structures, which are needed for these applications, are developed during annealing process above glass transition temperatures (T_g) of the blocks. Visualization of microphase separation patterns of block copolymers with AFM is trivial when hard tapping imaging is performed at temperature where one component is in glassy state, another – in rubbery-like. These both issues: annealing and visualization are illustrated by AFM images in Figures 23a–b. The phase images were obtained on a film triblock copolymer of polystyrene-block-polybutadiene-block-polystyrene (SBS) immediately after spin-casting and after intensive annealing. The differences of morphology of the samples are evident. The alternative lamellar structures

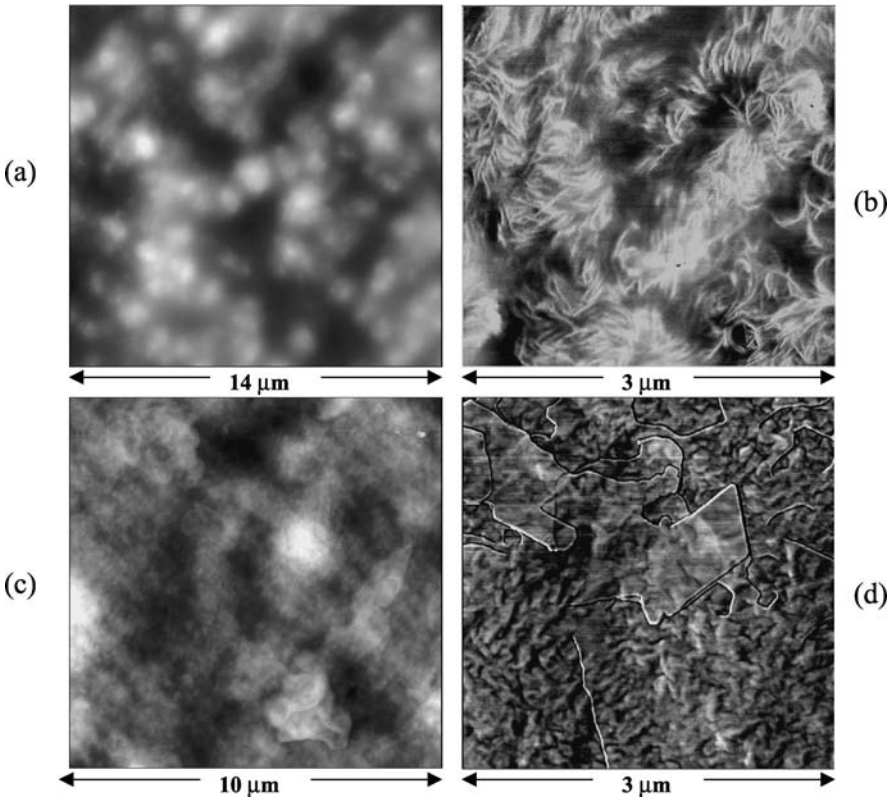

Figure 22. (a)–(b) Height and phase images of surface of linear low-density PE film. (c)–(d) Height and phase images of surface of low-density PE film.

belong to glassy polystyrene (PS) blocks, which have a bright contrast, and to rubbery polybutadiene (PB) blocks, which are recognized by darker contrast. Actually, the contrast between the components is strong at temperatures of around 100°C where softening of PS block occurs. Therefore, for some block copolymers, high-contrast imaging can be achieved at temperatures above the glass transition of one component but below the glass transition of another one [39].

An example of AFM characterization of bulk morphology of block copolymers is given in Figures 23c–d. These images were obtained on two cross-sections, which were made perpendicular and parallel to the main direction of a SBS rod, respectively. The rod was initially prepared with a viscosimeter and subjected to an extremely long term annealing. A well-ordered hexagonal pattern was detected in the AFM image of the perpendicular cross-section (Figure 23c) and the extended linear structures are seen in the image of the parallel cross-section (Figure 23d). These results unambiguously indicate that the perfect packing of polystyrene and polybutadiene cylinders was

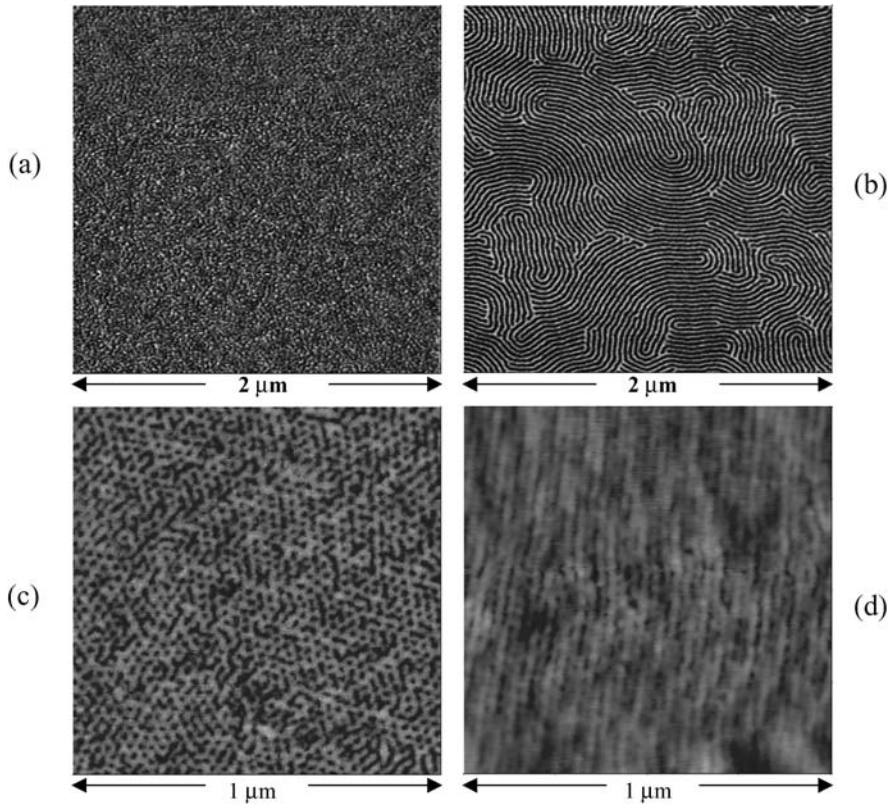

Figure 23. (a)–(b) Phase images of polystyrene-block-polybutadiene-block-polystyrene (SBS) film just after spin casting and after high-temperature annealing, respectively. (c)–(d) Phase image of cross-sections of an annealed SBS rod, which were made perpendicular and parallel to the rod main direction.

achieved in this material. As in the case of the SBS film, the dark spots in the image in Figure 23c correspond to PB cylinders and the bright spots – to PS [40].

Polymer Blends and Nanocomposites

Multicomponent rubber-like materials are often explored with AFM to tackle various problems of morphology of elastomer blends, partially cross-linked materials and visualization of filler [carbon black (CB), silica, clay particles, oil, etc] distribution, [41, 42]. Oil is usually incorporated in high viscous elastomers matrix to improve the material rheology and decreases the cost as well. Here we present the results of the ongoing study of morphology alterations of ethylene-propylene-diene rubber (EPDM) loaded with oil, which is caused by cross-linking process. The phase image of uncured EPDM filled with oil exhibits the complex morphology of this material, Figure 24a. Dark locations are related to oil component and they are distributed through the sample either

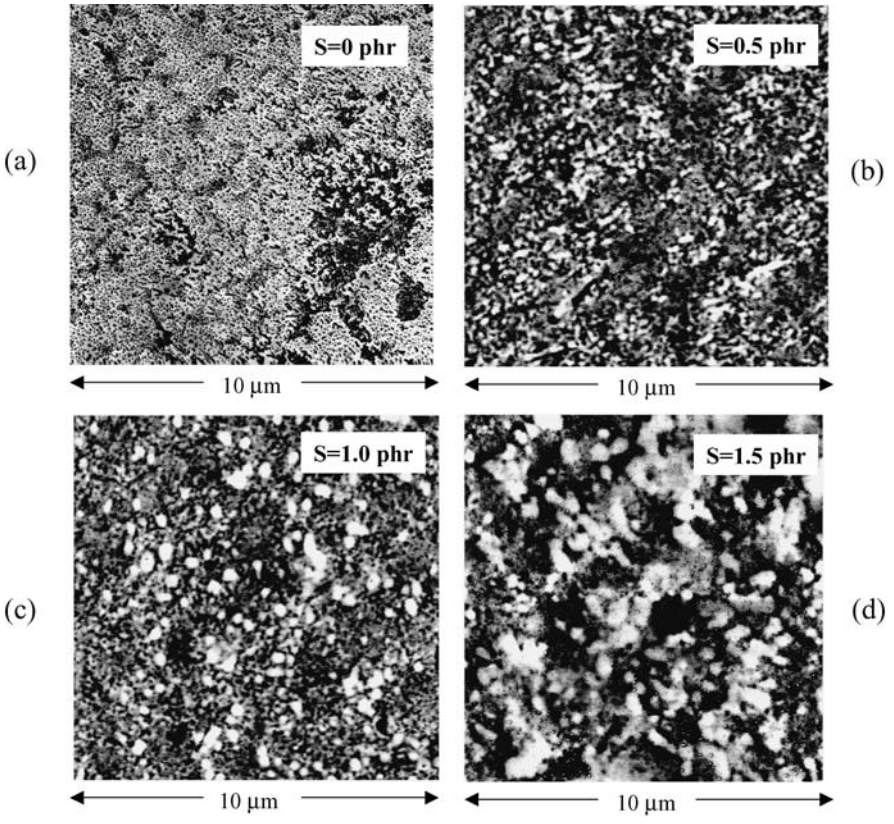

Figure 24. Phase images of EPDM rubber loaded with oil in an uncured state (a) and after curing with different amount of sulfur: S = 0.5 phr – (b), S = 1.0 phr – (c) and S = 1.5 phr – (d).

as homogeneously spread nanoscale inclusions or as larger clusters of various size and shape. Bright domains, which appear in the images of the samples after curing, represent the cross-linked rubber material. With the increase of concentration of curing agent (sulfur) from 0.5 phr to 1.0 phr the size of these domains enlarges from 52 to 82 nm, Figures 24b–c. As sulfur content increased further (S = 1.5 phr), the cross-linked material is seen as aggregates of 100–200 nm in size, and they occupied 28% of the image area, Figure 24d. This is twice more than the 13% area coverage by the cured rubber at S = 0.5 phr. that is twice large than in Figure 24b.

New engineering materials—thermoplastic vulcanizates (TPV) are more easily processed than traditional cross-linked rubbers but exhibit similar performance. They are essentially blends of rubber components with plastics, which are loaded with different fillers. Therefore, analysis of morphology of such TPV is helpful for optimization of their performance. Electrically conducting TPV, which are filled by CB particles, are can be used as sensors, switches, and electromagnetic shields. A percolation threshold

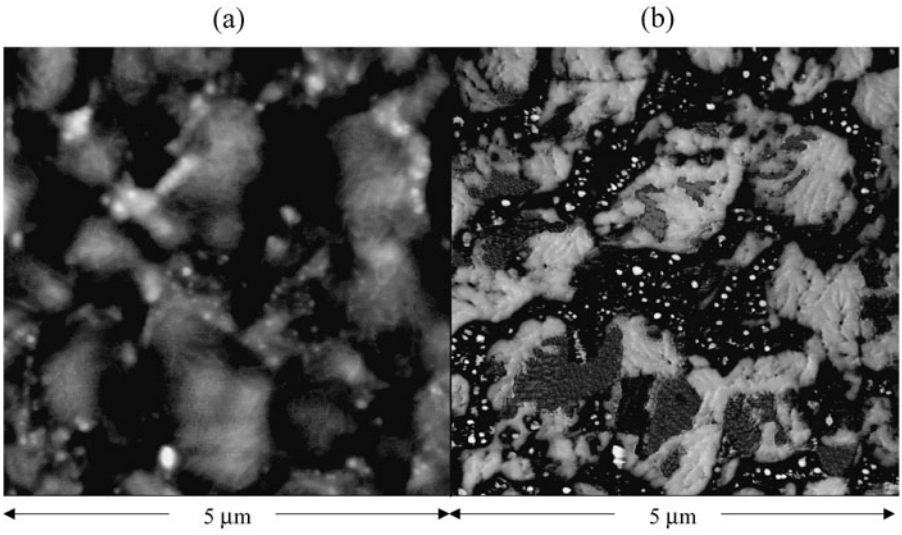

Figure 25. (a)–(b) Height and phase images of thermoplastic vulcanizate made by mixing EPDM, isotactic polypropylene and carbon black.

in these materials could be reached at small CB loading because of selective localization of these conducting particles in one of the components or at the interfaces. Electric force microscopy (EFM) in also attracted for imaging of CB particles [43]. Height and phase images in Figures 25a–b show morphology of the material made of isotactic polypropylene (iPP), EPDM and CB. The distribution of individual components is well distinguished in the phase image. The bright patches are allocated to EPDM domains in which the contrast variations point to locations with different cross-linking density. There are no indications of the presence of CB particles in the rubber domains. The darker regions with 40–50 nm bright particles represent iPP domains filled by CB. The described morphology has been the result of the optimization of mixing conditions and allows achieving low specific resistance (2.5 Ohm × cm) with minimal CB loading.

Composite materials with filler particles of tens and hundreds of nanometers in size are known and utilized for a long time. Recent attention to such composite materials has been motivated by research efforts to design nanocomposites with improved mechanical, adhesion, thermal and other properties. Polymers filled with mineral layered materials, such as different clays, graphite, etc. are of special interest. One of the possible developments in these systems is based on exfoliation of clay clusters into individual sheets of molecular thickness. Success of these efforts will give considerable increase of the filler surface that will impact properties, which depend on polymer-filler interfacial interactions. The intercalation and exfoliation processes can be monitored with high-resolution TEM and AFM that offer visualization of the clay particles and their individual sheets. Two AFM images of the polymer nanocomposite are presented

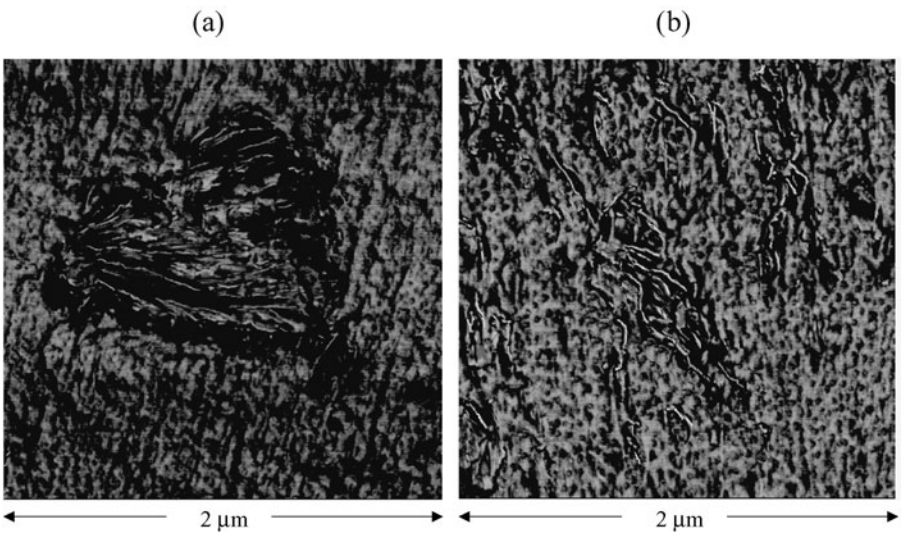

Figure 26. (a)–(b) Phase images of nanocomposite prepared of polypropylene and clay particles.

in Figures 26a–b. The images were obtained on a microtomed surface and the first of them shows a clay particle with multilayer morphology. The sample location with individual clay sheets, which are seen as edge-on structures of 40–50 nm in width, is presented in the second image. This morphology hints on successful exfoliation of the clay particles. There are several issues of sample preparation and optimization of imaging of extremely thin filler layers that should be considered in interplay between AFM and TEM.

Biomaterials are one of the fast growing areas where AFM role for material characterization will increase substantially. Obviously, dealing with materials, which performance includes interactions with living tissue and circulating blood in physiological conditions, will be more challenging for characterization. Therefore, there are a lot of hurdles to overcome, and we are just at the beginning. First steps are already made and AFM imaging of biological objects is quite established field, and there is also knowledge in studies of polymer materials, which are often used as biomaterials. Example of AFM studies of biomaterial is give by images in Figures 27a–b. These images were obtained on surface of felt matrix, which is prepared by mixing collagen and hyaluronic acid (HyA). The felt is employed for connective tissues repair and cosmetic purposes [44]. The large-scale morphology in Figure 27a shows an extended collagen aggregate incorporated into HyA. The later is recognized by dendritic morphology, which is formed of fibrilar strands. The phase image in Figure 27b demonstrates the details of the collagen aggregates, which is built of individual collagen. Collagen is a triple helix object with 300 × 1.5 nm dimensions, which consists of three extended protein chains that wrap around one another [45, 46]. The collagen molecules are also exhibit 60 nm pitch. The fact that similar pitch is observed in the extended aggregate

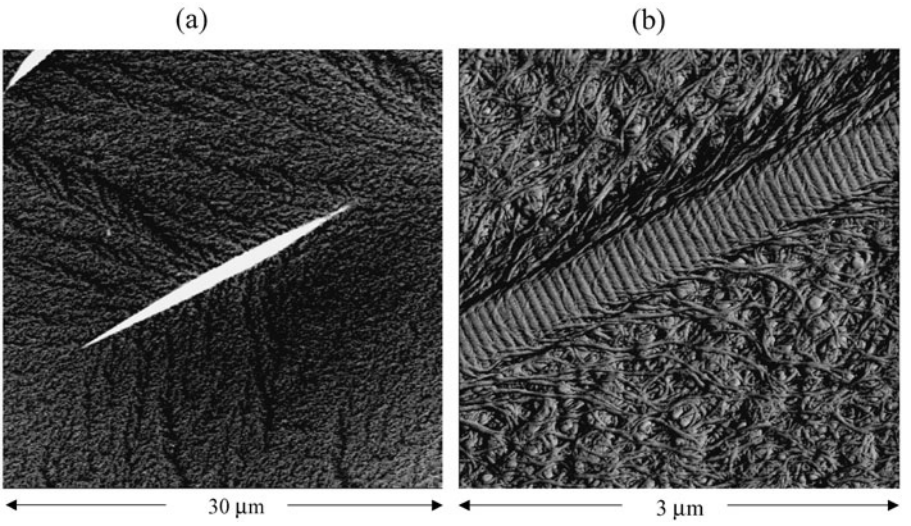

Figure 27. (a)–(b) Height and phase images of a surface of felt matrix prepared by mixing collagen and hyaluronic acid.

(Figure 26b) implies the ordered stacking of individual collagen molecules forming this structure. In addition, one sees a large number of thin strands unwinding from the aggregate into the nearby surface regions. This architecture helps of the collagen incorporation into the HyA matrix.

CONCLUDING REMARKS

Atomic force microscopy is the leading scanning probe technique and has become important in characterization of materials at the sub-micron scale. A principle AFM application is making high-resolution 3-dimensional images of surface topography. The examination of roughness of manufactured surfaces and accurate control of microscopic patterns are two important areas of industrial AFM applications. The unbeatable force sensitivity and nm-scale resolution of AFM is likely to make it practically the exclusive method for evaluation of sub-100-nm structures that will be the essence of nanotechnology. Ongoing development of softer and shaper probes will empower this technique further. This progress will enhance image resolution and will improve control over tip-sample forces at lower force level thus allow imaging of extremely soft materials impossible to date. In addition to high-resolution imaging, compositional mapping is recognized as the key feature for the majority of applications in studies of soft materials such as polymers and biological objects. The examples collected in this chapter support this conclusion. Further expansion of AFM experimental data is expected with a broader use of temperature and environmental accessories.

Progress is also expected in local measurements of mechanical properties. There are a number of different approaches (force modulation, oscillatory shearing, nanoindentation, etc.), which are applied for this purpose. These techniques provide semiquantitative data in a relatively narrow frequency range, mostly around resonant frequencies of the piezoactuators or probes. Although such measurements are extremely important they should be extended to a broader frequency range over several decades of frequencies where molecular motion and relaxation of macromolecules take place. Such studies of polymer viscoelastic behavior have become important not only for macroscopic samples but also for functional plastic and rubbery-like structures and elements with dimensions in the millimeter and micron range. Measurements at those scales should be performed with AFM–related techniques. The demand for such studies will further increase with development of nanotechnology.

The probing of materials with AFM is basically realized through mechanical interactions. Therefore, only indirect correlation between these measurements and chemical nature of a sample or its constituents can be derived from such studies. This does not fulfill the need of compositional analysis with chemical identification. The latest achievements in this field are primarily related with soft X-ray microscopy, which provide chemically sensitive mapping with resolution of tens nanometers [65]. Yet this technique requires the use of synchrotron radiation sources. Conventional methods like FTIR-microscopy provides chemical mapping only with resolution of several microns. Recently, a combination of AFM and infrared spectrometry has been successfully applied to collecting IR spectra of polymers from the tip-sample junction [66]. In perspective, such a combination might become an extremely powerful mapping technique with lateral resolution in the tens of nanometers range.

REFERENCES

1. G. Binnig, H. Rohrer, Ch. Gerber and E. Weibel, *Phys. Rev. Lett*. 49 (1982), 57.
2. G. Binnig, C. Quate and Ch. Gerber, *Phys. Rev. Lett*. 56 (1986), 930.
3. S. Alexander, US Patent 4,369,657, filed July 25, 1981.
4. S. Alexander, L. Hellemans, O. Marti, J. Schneir, V. Elings, P. K. Hansma, M. Longmire and J. Gurley, *J. Appl. Phys.* 65 (1989), 164.
5. Y. Miyahara, M. Deschler, T. Fujii, S. Watanabe and H. Bleuler, *Appl. Surf. Sci*. 18 (2002), 450.
6. Q. Zhong, D. Innis, K. Kjoller and V. B. Elings Surf. Sci. Let. 290 (1993) L688.
7. D. Klinov and S. Magonov, *Appl. Phys. Lett*. 84 (2004), 2697.
8. The diamond probes are made by B. Mesa, MicroStar Technology, Huntsville, TX, USA, www.microstartech.com.
9. H. J. Dai, J. H. Hafner, A. G. Rinzler, D. T. Colbert and R. E. Smalley, *Nature* 384 (1996) 147.
10. J. H. Hafner, C. L. Cheung and C. M. Lieber, *Nature* 398 (1999), 761.
11. C. Su and S. Magonov, Patent Application, USA (2003).
12. R. Pechmann, J. M. Koehler, W. Fritzsche, A. Schaper and T. V. Jovin, *Rev. Sci. Instr.* 65 (1994) 3702.
13. S. N. Magonov and M.-H. Whangbo, *Surface Analysis with STM and AFM*, VCH, Weinheim (1996).
14. P. Mailvald, H.-J. Butt, S. A. C. Gould, C. B. Prater, B. Drake, V. Elings and P. K. Hansma, *Nanotechnology* 2 (1991), 103.
15. A. L. Weisenhorn, P. Maivald, H.-J. Butt and P. K. Hansma, Phys. Rev. B. 45 (1992) 11226.
16. D. Chernoff and S. Magonov in: *Comprehensive Desk Reference of Polymer Characterization and Analysis*, R. F. Brady, Jr. (Ed.) pp. 490–531ACS, Oxford Press, 2003.
17. U. Landman, W. D. Luedke and A. Nitzan, *Surf. Sci. Lett*. 10 (1989), L177.
18. F. J. Giessibl, *Science* 267 (1995), 68.

19. Mohler, C. E., Landes, B. G., Meyers G. F., Kern, B. J., Oullette K. B., Magonov S. N. AIP Conference Proceedings 683 Characterization and Metrology for ULSI: 2003 International Conference, D. G. Seiler et. al. (Eds.) pp. 562–566 American Institute of Physics, New York (2003).
20. F. Y. Hansen, L. W. Bruch and H. Taub, *Phys. Rev. B* 54 (1996), 14077.
21. S. N. Magonov, N. Yerina, G. Ungar and D. Ivanov, in preparation (2004).
22. D. A. Ivanov, R. Daniels, and S. N. Magonov, *Exploring the High-Temperature AFM and Its Use for Studies Polymers*, Application Note published by Digital Instruments/Veeco Metrology Group (2001). URL: http://www.veeco.com/appnotes/AN45_HeatingStage.pdf
22. S. A. Ponomarenko, N. I. Boiko, V. P. Shibaev and S. N. Magonov, *Langmuir* 16 (2000), 5487.
23. Yu. K. Godovsky and S. N. Magonov, *Langmuir* 16 (2000), 3549.
24. D. A. Ivanov, Z. Amalou and S. N. Magonov, *Macromolecules* 34 (2001) 8944.
25. Yu. K. Godovsky, V. S. Papkov and S. N. Magonov, *Macromolecules* 34 (2001), 976.
26. J. Kumaki, Y. Nishikawa and T. Hashimoto, *JACS* 118 (1996), 3321.
27. S. S. Sheiko and M. Möller, *Chem. Revs* 101 (2001), 4099.
28. M. Gerle, K. Fischer, M. Schmidt, S. Roos, A. H. E. Mueller, S. S. Sheiko, S. A. Prokhorova and M. Möller, *Macromolecules* 32 (1999), 2629.
29. V. Percec, M. N. Holerca, S. N. Magonov, D. J. P. Yeardley, G. Ungar, H. Duan and S. D. Hudson, *Biomacromolecules* 2 (2001), 706.
30. S. Magonov in: *Applied Scanning Probe Techniques*, H. Fuchs, M. Hosaka and B. Bhushan (Eds.) pp. 207–251, Springer, Berlin, 2004.
31. S. Magonov and N. Yerina, *Langmuir* 19 (2003), 504.
32. S. N. Magonov, N. A. Yerina, G. Ungar, D. H. Reneker and D. A. Ivanov, *Macromolecules* 36 (2003), 5637.
33. G. Ungar and X. Zeng, *Chem. Revs*. 101 (2001), 4157.
34. P. H. Geil, *Polymer Single Crystals*, John Willey & Sons, New York, (1963).
35. S. N. Magonov, N. A. Yerina and D. H. Reneker, *Macromolecules* (2004), submitted.
36. S. N. Magonov and Yu. Godovsky, *Amer. Lab.* (31) 1999 , 52.
37. G. L. Gaines, *Langmuir* 7 (1991), 3054.
38. M. Maaloum, P. Muller and M. P. Kraft, *Angew. Chem* 114 (2002), 4507.
39. M. J. Fasolka, A. M. Mayes and S. Magonov, *Ultramicroscopy* 90 (2001), 2.
40. S. N. Magonov, V. Elings, J. Cleveland, D. Denley and M.-H. Whangbo, *Surface Science* 389 (1997), 201.
41. A. A. Galuska, R. R. Poulter and K. O. McElrath, *Surface and Interface Analysis* 25 (1997) 418.
42. N. A. Yerina and S. N. Magonov S. N., *Rubber Industry and Technology* 76 (2003) 846.
43. R. Viswanathan and M. B. Heaney, *Phys. Rev. Lett*. 75 (1995), 4433.
44. C. J. Doillon, C. F. Whyne, S. Brandwein and F. H. Silver, *J. Biomed. Mater. Res.* 20 (1986), 1219.
45. K. A. Piez, in: *Encyclopedia of Polymer Science and Engineering*, Vol. 3, p. 699. Willey, New York (1985).
46. H. Yokota, F. Johnson, H. Lu, R. M. Robinson, A. M. Belu, M. D. Garrison, B. D. Ratner, J. Trask, D. L. Miller, *Nucleic Acids Research* 25 (1997), 1064.